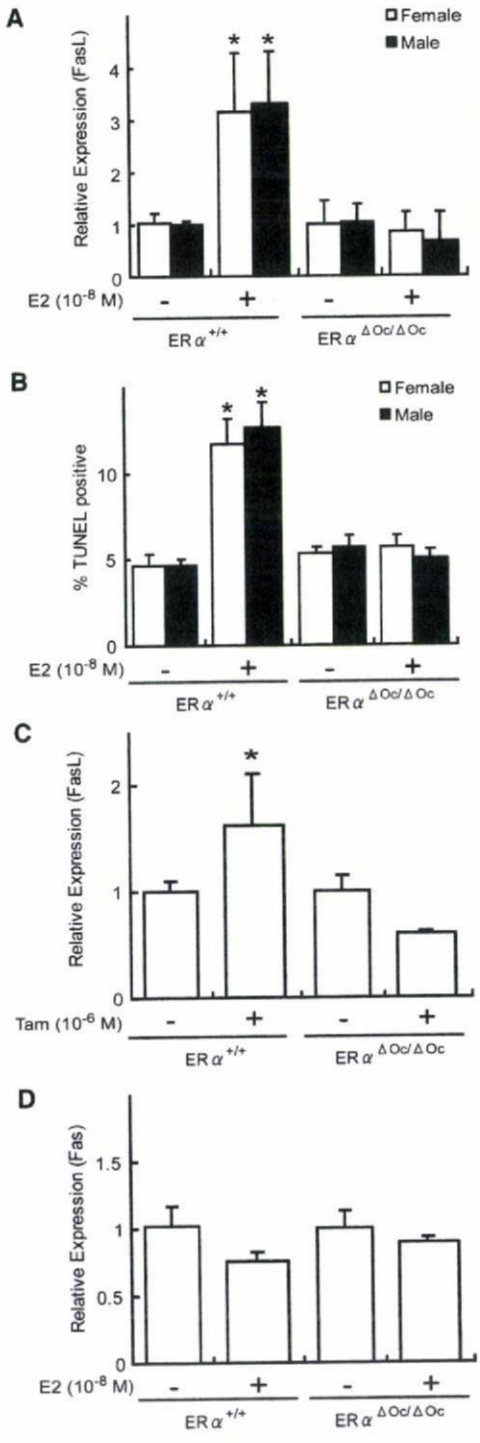

Figure 7. Estrogen-Induced *FasL* Expression and Apoptosis Required ERα in Cultured Osteoclasts

(A) Real-time RT-PCR analysis of *FasL* expression using total RNA obtained from in vitro primary cultured osteoclasts of each genotype at 3 days after RANKL stimulation, treated with or without E2 (10^{-8} M) for 4 hr (*$p < 0.05$ compared to the group treated without E2). Data are represented as mean ± SEM.

(B) Apoptotic cells were defined as those with TUNEL-positive nuclei among TRAP-positive multinucleated primary cultured osteoclasts treated with or without E2 (10^{-8} M) for 12 hr in 96-well plates (*$p < 0.05$ compared to the group treated without E2). Data are represented as mean ± SEM.

(C) *FasL* expression in each genotypic female osteoclastic cells treated with or without Tam (10^{-6} M) (*$p < 0.05$ compared to the group treated without Tam). Data are represented as mean ± SEM.

(D) Expression of *Fas* was measured as described in the legend of Figure 7A. Data are represented as mean ± SEM.

markedly elevated levels of testosterone in ERα KO females may be potent enough to maintain normal bone turnover (Syed and Khosla, 2005), it is likely that the activated AR might be functionally sufficient in male mice to compensate for the ERα deficiency in bone (Kawano et al., 2003). However, species differences in the osteoprotective action of sex steroid hormones still need to be carefully addressed.

Fas/FasL system-mediated apoptotic induction of osteoclasts by estrogen may well be a part of the mechanism for the antiresorptive action of estrogen and SERMs in trabecular bone areas (Delmas, 2002; Rodan and Martin, 2000; Simpson and Davis, 2001; Syed and Khosla, 2005; Tolar et al., 2004). Regulation of osteoclast differentiation is tightly coupled to osteoblastic function in terms of cytokine production and cell-cell contact (Karsenty and Wagner, 2002; Martin and Sims, 2005; Mundy and Elefteriou, 2006; Teitelbaum and Ross, 2003). Indeed, upregulation of osteoclastogenic cytokines by ovariectomy was unaffected in $ER\alpha^{\Delta Oc/\Delta Oc}$ females. Considering the observation that cortical bone mass is increased in ovariectomized $ER\alpha^{\Delta Oc/\Delta Oc}$ females during estrogen treatment, it is conceivable that the antiresorptive estrogen action in cortical bone is also mediated by osteoblastic ERα. In this regard, FasL induction by estrogen in osteoblasts may contribute to the osteoprotective estrogen action, and *FasL* gene induction by estrogen was in fact detected in primary cultured osteoblasts from female calvaria by us as well as another group (S. Krum and M. Brown, personal communication). Thus, similar experiments in which ERα is selectively ablated in osteoblasts are needed to define the role of ERα in these cells.

In osteoclastic cells, expression of the *FasL* gene, which leads to apoptosis, appears to be positive controlled by activated ERα. Not surprisingly, a direct binding site for ERα has been mapped in the *FasL* gene locus (S. Krum and M. Brown, personal communication). An osteoclast- and cell-differentiation stage-specific mechanism may underlie this gene induction in the *FasL* gene promoter. A recent study demonstrated that ERα recruitment to specific promoter sites of given ERα target genes was cell-type specific (Carroll et al., 2005). Thus, there is significant impetus to identify the osteoclastic factor that associates with ERα in the *FasL* gene promoter. Such identification will lead to a better understanding of the molecular basis of the osteoprotective estrogen action and provide a target against which to develop SERMs of greater effectiveness.

EXPERIMENTAL PROCEDURES

Ctsk-Cre Construction and Generation of the Knockin Mouse Lines

An RP23-422n18 BAC clone containing the mouse *Ctsk* gene was purchased from Invitrogen (Carlsbad, CA). The *FRT-Kan^r/Neo^r-FRT* and *nlsCre* fragments were obtained from plasmids pSK2/3-*FRT-Neo* and pIC-*Cre*. Two homologous arms of 500 bp from the *Ctsk* gene were inserted into both sides of the *nlsCre-FRT-Kan^r/Neo^r-FRT* cassette in the pSK2/3-*FRT-Neo* plasmid. The *nlsCre-FRT-Kan^r/Neo^r-FRT* cassette was introduced into the endogenous ATG start site of the *Ctsk* gene by recombineering approaches (Copeland et al., 2001). Targeted BAC was reduced in size from 189 kb to 26 kb and subcloned into the pMC1-DTpA vector by the gap-repair method. The targeted TT2 ES clones were selected after positive-negative selection with G418 and DT-A with Southern analysis, then aggregated with single eight-cell embryos from CD-1 mice (Yoshizawa et al., 1997). Chimeric mice were then crossed with a general deleter mouse line, *ACTB-Flpe* (Jackson Laboratory), to remove the *Kan^r/Neo^r* cassette. The *Ctsk-Cre* mice (*Ctsk$^{Cre/+}$*), originally on a hybrid C57BL/6 and CBA genetic background, were backcrossed for four generations into a C57BL/6J background. *FasL$^{gld/gld}$* mice were also purchased from Jackson Laboratory.

Analysis of Cre Recombinase Activities

Expression of the Cre transcript was detected by RT-PCR. Southern analysis using a *Cre* cDNA probe was performed with total RNA extracted from 12-week-old mice. To evaluate the specificity and efficiency of Cre-mediated recombination, we mated the *Ctsk$^{Cre/+}$* mice to *CAG-CAT-Z* reporter mice (kindly provided by J. Miyazaki) (Sakai and Miyazaki, 1997) and genotyped their offspring with *Cre*-specific primers. β-galactosidase activity of the expressed *LacZ* gene driven by the *CAG* promoter was expected to be detected in the given cells expressing functional Cre recombinase.

In Vitro Osteoclastogenesis and Ligand Application

Bone-marrow cells derived from 8-week-old mice were plated in culture dishes containing α-MEM (GIBCO-BRL) with 10% FBS (JRH) and 10 ng/ml M-CSF (Genzyme). After incubation for 48 hr, adherent cells were used as osteoclast precursor cells after washing out the nonadherent cells. Cells were cultured in the presence of 10 ng/ml M-CSF and 100 ng/ml RANKL (Peprotech) to generate osteoclast-like cells (Koga et al., 2004) for 3 days, so the total culture time was 5 days. Three days after RANKL stimulation, primary cultured osteoclasts were treated with 10^{-8} M of 17β-estradiol (E2) (Sigma-Aldrich Co.) or 10^{-6} M 4-hydroxytamoxifen (Tam) (Sigma-Aldrich Co.) in phenol-red free medium.

Generation of Osteoclast-Specific ERα KO Mice

The ERα conditional (*ERα$^{flox/flox}$*) (Dupont et al., 2000) and null alleles with a C57BL/6J background have been previously described. *ERα$^{flox/flox}$* mice were crossed with *Ctsk$^{Cre/+}$* mice to generate *Ctsk$^{Cre/+}$; ERα$^{flox/+}$* mice. *Ctsk$^{Cre/+}$; ERα$^{+/+}$* (*ERα$^{+/+}$*) and *Ctsk$^{Cre/+}$; ERα$^{flox/flox}$* (*ERα$^{\Delta Oc/\Delta Oc}$*) mice were obtained by crossing *Ctsk$^{Cre/+}$; ERα$^{flox/+}$* with *ERα$^{flox/+}$* mouse lines.

Radiological Analysis

Bone radiographs of the femurs of 12-week-old *Ctsk$^{Cre/+}$; ERα$^{flox/flox}$* (*ERα$^{\Delta Oc/\Delta Oc}$*) and *Ctsk$^{Cre/+}$; ERα$^{+/+}$* (*ERα$^{+/+}$*) littermates were visualized with a soft X-ray apparatus (TRS-1005: SOFTRON). BMD was measured by DXA using a bone mineral analyzer (DCS-600EX: ALOKA). Micro Computed Tomography scanning of the femurs was performed using a composite X-ray analyzer (NX-CP-C80H-IL: Nittetsu ELEX Co.) (Kawano et al., 2003). Tomograms were obtained with a slice thickness of 10 μm and reconstructed at 12 × 12 pixels into a 3D image by the volume-rending method (VIP-Station; Teijin System Technology) using a computer.

Analysis of Skeletal Morphology

Twelve-week-old *Ctsk$^{Cre/+}$; ERα$^{flox/flox}$* (*ERα$^{\Delta Oc/\Delta Oc}$*) and *Ctsk$^{Cre/+}$; ERα$^{+/+}$* (*ERα$^{+/+}$*) littermates were double labeled with subcutaneous injections of 16 mg/kg of calcein (Sigma) at 4 and 2 days before sacrifice. Tibiae were removed from each mouse and fixed with 70% ethanol. They were stained with Villanueva bone stain for 7 days and embedded in methyl-methacrylate (Wako) (Yoshizawa et al., 1997). Frontal plane sections (5-μm thick) of the proximal tibia were cut using a Microtome (LEICA). The cancellous bone was measured in the secondary spongiosa located 500 μm from the epiphyseal growth plate and 160 μm from the endocortical surface (Kawano et al., 2003; Nakamichi et al., 2003). Bone histomorphometric measurements of the tibia were made using a semiautomatic image analyzing system (System Supply) and a fluorescent microscope (Optiphot; Nikon). Similar measurements of the lumbar vertebral bodies were done as previously reported (Takeda et al., 2002). Standard bone histomorphometrical nomenclatures, symbols, and units were used as described in the report of the ASBMR Histomophometry Nomenclature Committee.

Ovariectomy and Hormone Replacement

Female *Ctsk$^{Cre/+}$; ERα$^{flox/flox}$* (*ERα$^{\Delta Oc/\Delta Oc}$*) and *Ctsk$^{Cre/+}$; ERα$^{+/+}$* (*ERα$^{+/+}$*) littermates were ovariectomized or sham operated at 8–12 weeks of age for 2 weeks for all experiments, and slow releasing pellets of E2 (0.83 μg/day) or placebo (Innovative Research, Sarasota, FL) were implanted subcutaneously in the scapular region behind the neck (Sato et al., 2004; Shiina et al., 2006).

Immunohistochemistry

Twelve-week-old *Ctsk$^{Cre/+}$; ERα$^{flox/flox}$* (*ERα$^{\Delta Oc/\Delta Oc}$*) and *Ctsk$^{Cre/+}$; ERα$^{+/+}$* (*ERα$^{+/+}$*) littermates were fixed with 4% PFA by perfusion. Serial sections of the brain (20 μm thick) were divided into two groups and used for single labeling for the ERα or thionin to allow determination of the areas to be measured. Tibiae and femurs were decalcified in 10% EDTA for 2–4 weeks after fixation and then embedded in paraffin sections. Sections were incubated in L.A.B. solution (Polysciences) for 30 min to retrieve antigen. The cooled sections were incubated in 1% H_2O_2 for 30 min to quench endogenous peroxidase and then washed with 1% Triton X-100 in PBS for 10 min. To block nonspecific antibody binding, sections were incubated in blocking solution (DAKO) for 5 min. Sections were then incubated with anti-ERα (Santa Cruz, CA) and anti-FasL (Santa Cruz, CA) in blocking solution overnight at 4°C. Staining was then performed using the EnVision+ HRP System (Dako) and 3, 3'-diaminobendizine tetrahydrochloride substrate (Sigma), counterstained with TRAP, dehydrated through an ethanol series and xylene, before mounting (Sato et al., 2004).

ERα Overexpression

Two days after RANKL stimulation, an expression vector of mouse ERα was tranfected into immature osteoclastic cells from *ERα$^{\Delta Oc/\Delta Oc}$* mice using Superfect (QIAGEN) as manufacture's instruction.

Real-Time RT-PCR

One microgram of total RNA from each sample was reverse transcribed into first-strand cDNA with random hexamers using Superscript III reverse transcriptase (Invitrogen). Primer sets for all genes were purchased from Takara Bio. Inc. (Tokyo, Japan). Real-time RT-PCR was performed using SYBR Premix Ex Taq (Takara) with the ABI PRISM 7900HT (Applied Biosystems) according to the manufacturer's instructions. Experimental samples were matched to a standard curve generated by amplifying serially diluted products using the same PCR protocol. To correct for variability in RNA recovery and efficiency of reverse transcription, *Gapdh* cDNA was amplified and quantified in each cDNA preparation. Normalization and calculation steps were performed as reported previously (Takezawa et al., 2007).

TUNEL/TRAP Staining

The TUNEL method was performed using the ApopTag Fluorescein In Situ Apoptosis Detection Kit (CHEMICON international) according to the manufacturer's instructions with a slight modification. This was followed by TRAP staining as previously reported (Kobayashi et al., 2000).

Cytokine Assays

Bone marrow and blood were collected at 2 weeks after sham operation or ovariectomy. Bone-marrow cells were cultured for 3 days in DMEM. The levels of TNFα, IL-1α, and IL-6 in the culture media and serum RANKL were determined by ELISA (R&D Systems).

Western Blot

Osteoclast precursor cells were treated with or without 100 ng/ml of soluble RANKL. After 15 minutes, cell extracts were harvested from the cells using lysis buffer containing 100 mM Tris-HCl (pH 7.8), 150 mM NaCl, 0.1% Triton X-100, 5% protease inhibitor cocktail (Sigma), and 5% phosphatase inhibitor cocktail (Sigma). An equivalent amount of protein from each of the cell extracts and proteins of femoral bone extracted using ISOGEN was loaded for SDS-PAGE and transferred to PVDF membranes (Amersham Biosciences). The membranes were developed with enhanced chemiluminescence reagent (Amersham Biosciences) (Ohtake et al., 2003). Phosphorylation of p38 MAPK and IκB were evaluated using antibodies purchased from Cell Signaling Technology (Koga et al., 2004) and anti-FasL antibody was purchased from Santa Cruz Biotechnology (sc-834).

Actin-Ring Formation

Cells were fixed for 15 min in warm 4% paraformaldehyde (PFA). After fixation, cells were washed three times with PBS with 0.1% Triton X-100 (PBST) and incubated with 0.2 U/ml rhodamine phalloidin (Molecular Probes) for 30 min and washed again three times in PBST.

Statistical Analysis

Data were analyzed by two-tailed student's t test. For all graphs, data are represented as mean ± SEM.

Supplemental Data

Supplemental Data include Supplemental Experimental Procedures and four figures and can be found with this article online at http://www.cell.com/cgi/content/full/130/5/811/DC1/.

ACKNOWLEDGMENTS

We thank Drs. S. Krum and M. Brown to share with their unpublished results; Drs. K. Yoshimura, Y. Nakamichi, T. Watanabe, J. Miyamoto, H. Shiina, T. Fukuda, Ms. Y. Sato, and S. Tanaka for generation of the KO mice; Drs. T. Koga, H. Takagi, E. Ochiai, and N. Moriyama for technical help; Dr. J. Miyazaki for *CAG-CAT-Z* reporter mice, and H. Higuchi and K. Hiraga for manuscript preparation. This work was supported in part by priority areas from the Ministry of Education, Culture, Sports, Science and Technology (to S.K.) and the Program for Promotion of Basic Research Activities for Innovative Biosciences (PROBRAIN).

Received: February 23, 2007
Revised: May 21, 2007
Accepted: July 17, 2007
Published: September 6, 2007

REFERENCES

Belandia, B., and Parker, M.G. (2003). Nuclear receptors: a rendezvous for chromatin remodeling factors. Cell *114*, 277–280.

Bland, R. (2000). Steroid hormone receptor expression and action in bone. Clin. Sci. (Lond.) *98*, 217–240.

Carroll, J.S., Liu, X.S., Brodsky, A.S., Li, W., Meyer, C.A., Szary, A.J., Eeckhoute, J., Shao, W., Hestermann, E.V., Geistlinger, T.R., et al. (2005). Chromosome-wide mapping of estrogen receptor binding reveals long-range regulation requiring the forkhead protein FoxA1. Cell *122*, 33–43.

Chien, K.R., and Karsenty, G. (2005). Longevity and lineages: toward the integrative biology of degenerative diseases in heart, muscle, and bone. Cell *120*, 533–544.

Copeland, N.G., Jenkins, N.A., and Court, D.L. (2001). Recombineering: a powerful new tool for mouse functional genomics. Nat. Rev. Genet. *2*, 769–779.

Couse, J.F., and Korach, K.S. (1999). Estrogen receptor null mice: what have we learned and where will they lead us? Endocr. Rev. *20*, 358–417.

Delmas, P.D. (2002). Treatment of postmenopausal osteoporosis. Lancet *359*, 2018–2026.

Dupont, S., Krust, A., Gansmuller, A., Dierich, A., Chambon, P., and Mark, M. (2000). Effect of single and compound knockouts of estrogen receptors alpha (ERalpha) and beta (ERbeta) on mouse reproductive phenotypes. Development *127*, 4277–4291.

Gowen, M., Lazner, F., Dodds, R., Kapadia, R., Feild, J., Tavaria, M., Bertoncello, I., Drake, F., Zavarselk, S., Tellis, I., et al. (1999). Cathepsin K knockout mice develop osteopetrosis due to a deficit in matrix degradation but not demineralization. J. Bone Miner. Res. *14*, 1654–1663.

Harada, S., and Rodan, G.A. (2003). Control of osteoblast function and regulation of bone mass. Nature *423*, 349–355.

Kameda, T., Mano, H., Yuasa, T., Mori, Y., Miyazawa, K., Shiokawa, M., Nakamaru, Y., Hiroi, E., Hiura, K., Kameda, A., et al. (1997). Estrogen inhibits bone resorption by directly inducing apoptosis of the bone-resorbing osteoclasts. J. Exp. Med. *186*, 489–495.

Karsenty, G. (2006). Convergence between bone and energy homeostases: leptin regulation of bone mass. Cell Metab. *4*, 341–348.

Karsenty, G., and Wagner, E.F. (2002). Reaching a genetic and molecular understanding of skeletal development. Dev. Cell *2*, 389–406.

Kato, S., Ito, S., Noguchi, T., and Naito, H. (1989). Effects of brefeldin A on the synthesis and secretion of egg white proteins in primary cultured oviduct cells of laying Japanese quail (Coturnix coturnix japonica). Biochim. Biophys. Acta *991*, 36–43.

Kawano, H., Sato, T., Yamada, T., Matsumoto, T., Sekine, K., Watanabe, T., Nakamura, T., Fukuda, T., Yoshimura, K., Yoshizawa, T., et al. (2003). Suppressive function of androgen receptor in bone resorption. Proc. Natl. Acad. Sci. USA *100*, 9416–9421.

Kimble, R.B., Matayoshi, A.B., Vannice, J.L., Kung, V.T., Williams, C., and Pacifici, R. (1995). Simultaneous block of interleukin-1 and tumor necrosis factor is required to completely prevent bone loss in the early postovariectomy period. Endocrinology *136*, 3054–3061.

Kobayashi, Y., Hashimoto, F., Miyamoto, H., Kanaoka, K., Miyazaki-Kawashita, Y., Nakashima, T., Shibata, M., Kobayashi, K., Kato, Y., and Sakai, H. (2000). Force-induced osteoclast apoptosis in vivo is accompanied by elevation in transforming growth factor beta and osteoprotegerin expression. J. Bone Miner. Res. *15*, 1924–1934.

Koga, T., Inui, M., Inoue, K., Kim, S., Suematsu, A., Kobayashi, E., Iwata, T., Ohnishi, H., Matozaki, T., Kodama, T., et al. (2004). Costimulatory signals mediated by the ITAM motif cooperate with RANKL for bone homeostasis. Nature *428*, 758–763.

Li, C.Y., Jepsen, K.J., Majeska, R.J., Zhang, J., Ni, R., Gelb, B.D., and Schaffler, M.B. (2006). Mice lacking Cathepsin K maintain bone remodeling but develop bone fragility despite high bone mass. J. Bone Miner. Res. *21*, 865–875.

Mangelsdorf, D.J., Thummel, C., Beato, M., Herrlich, P., Schutz, G., Umesono, K., Blumberg, B., Kastner, P., Mark, M., Chambon, P., and Evans, R.M. (1995). The nuclear receptor superfamily: the second decade. Cell *83*, 835–839.

Martin, T.J., and Sims, N.A. (2005). Osteoclast-derived activity in the coupling of bone formation to resorption. Trends Mol. Med. *11*, 76–81.

Mueller, S.O., and Korach, K.S. (2001). Estrogen receptors and endocrine diseases: lessons from estrogen receptor knockout mice. Curr. Opin. Pharmacol. *1*, 613–619.

Mundy, G.R., and Elefteriou, F. (2006). Boning up on ephrin signaling. Cell *126*, 441–443.

Nakamichi, Y., Shukunami, C., Yamada, T., Aihara, K., Kawano, H., Sato, T., Nishizaki, Y., Yamamoto, Y., Shindo, M., Yoshimura, K., et al. (2003). Chondromodulin I is a bone remodeling factor. Mol. Cell. Biol. *23*, 636–644.

Ohtake, F., Takeyama, K., Matsumoto, T., Kitagawa, H., Yamamoto, Y., Nohara, K., Tohyama, C., Krust, A., Mimura, J., Chambon, P., et al. (2003). Modulation of oestrogen receptor signalling by association with the activated dioxin receptor. Nature *423*, 545–550.

Raisz, L.G. (2005). Pathogenesis of osteoporosis: concepts, conflicts, and prospects. J. Clin. Invest. *115*, 3318–3325.

Riggs, B.L., and Hartmann, L.C. (2003). Selective estrogen-receptor modulators–mechanisms of action and application to clinical practice. N. Engl. J. Med. *348*, 618–629.

Rodan, G.A., and Martin, T.J. (2000). Therapeutic approaches to bone diseases. Science *289*, 1508–1514.

Saftig, P., Hunziker, E., Wehmeyer, O., Jones, S., Boyde, A., Rommerskirch, W., Moritz, J.D., Schu, P., and von Figura, K. (1998). Impaired osteoclastic bone resorption leads to osteopetrosis in Cathepsin-K-deficient mice. Proc. Natl. Acad. Sci. USA *95*, 13453–13458.

Sakai, K., and Miyazaki, J. (1997). A transgenic mouse line that retains Cre recombinase activity in mature oocytes irrespective of the cre transgene transmission. Biochem. Biophys. Res. Commun. *237*, 318–324.

Sato, T., Matsumoto, T., Kawano, H., Watanabe, T., Uematsu, Y., Sekine, K., Fukuda, T., Aihara, K., Krust, A., Yamada, T., et al. (2004). Brain masculinization requires androgen receptor function. Proc. Natl. Acad. Sci. USA *101*, 1673–1678.

Shang, Y., and Brown, M. (2002). Molecular determinants for the tissue specificity of SERMs. Science *295*, 2465–2468.

Shiina, H., Matsumoto, T., Sato, T., Igarashi, K., Miyamoto, J., Takemasa, S., Sakari, M., Takada, I., Nakamura, T., Metzger, D., et al. (2006). Premature ovarian failure in androgen receptor-deficient mice. Proc. Natl. Acad. Sci. USA *103*, 224–229.

Simpson, E.R., and Davis, S.R. (2001). Minireview: aromatase and the regulation of estrogen biosynthesis–some new perspectives. Endocrinology *142*, 4589–4594.

Sims, N.A., Clement-Lacroix, P., Minet, D., Fraslon-Vanhulle, C., Gaillard-Kelly, M., Resche-Rigon, M., and Baron, R. (2003). A functional androgen receptor is not sufficient to allow estradiol to protect bone after gonadectomy in estradiol receptor-deficient mice. J. Clin. Invest. *111*, 1319–1327.

Smith, E.P., Boyd, J., Frank, G.R., Takahashi, H., Cohen, R.M., Specker, B., Williams, T.C., Lubahn, D.B., and Korach, K.S. (1994). Estrogen resistance caused by a mutation in the estrogen-receptor gene in a man. N. Engl. J. Med. *331*, 1056–1061.

Sun, L., Peng, Y., Sharrow, A.C., Iqbal, J., Zhang, Z., Papachristou, D.J., Zaidi, S., Zhu, L.L., Yaroslavskiy, B.B., Zhou, H., et al. (2006). FSH directly regulates bone mass. Cell *125*, 247–260.

Suzawa, M., Takada, I., Yanagisawa, J., Ohtake, F., Ogawa, S., Yamauchi, T., Kadowaki, T., Takeuchi, Y., Shibuya, H., Gotoh, Y., et al. (2003). Cytokines suppress adipogenesis and PPAR-gamma function through the TAK1/TAB1/NIK cascade. Nat. Cell Biol. *5*, 224–230.

Syed, F., and Khosla, S. (2005). Mechanisms of sex steroid effects on bone. Biochem. Biophys. Res. Commun. *328*, 688–696.

Takeda, S., Elefteriou, F., Levasseur, R., Liu, X., Zhao, L., Parker, K.L., Armstrong, D., Ducy, P., and Karsenty, G. (2002). Leptin regulates bone formation via the sympathetic nervous system. Cell *111*, 305–317.

Takezawa, S., Yokoyama, A., Okada, M., Fujiki, R., Iriyama, A., Yanagi, Y., Ito, H., Takada, I., Kishimoto, M., Miyajima, A., et al. (2007). A cell cycle-dependent co-repressor mediates photoreceptor cell-specific nuclear receptor function. EMBO J. *26*, 764–774.

Teitelbaum, S.L. (2006). Osteoclasts; culprits in inflammatory osteolysis. Arthritis Res. Ther. *8*, 201.

Teitelbaum, S.L. (2007). Osteoclasts: what do they do and how do they do it? Am. J. Pathol. *170*, 427–435.

Teitelbaum, S.L., and Ross, F.P. (2003). Genetic regulation of osteoclast development and function. Nat. Rev. Genet. *4*, 638–649.

Tolar, J., Teitelbaum, S.L., and Orchard, P.J. (2004). Osteopetrosis. N. Engl. J. Med. *351*, 2839–2849.

Windahl, S.H., Andersson, G., and Gustafsson, J.A. (2002). Elucidation of estrogen receptor function in bone with the use of mouse models. Trends Endocrinol. Metab. *13*, 195–200.

Yoshizawa, T., Handa, Y., Uematsu, Y., Takeda, S., Sekine, K., Yoshihara, Y., Kawakami, T., Arioka, K., Sato, H., Uchiyama, Y., et al. (1997). Mice lacking the vitamin D receptor exhibit impaired bone formation, uterine hypoplasia and growth retardation after weaning. Nat. Genet. *16*, 391–396.

Zaman, G., Jessop, H.L., Muzylak, M., De Souza, R.L., Pitsillides, A.A., Price, J.S., and Lanyon, L.L. (2006). Osteocytes use estrogen receptor alpha to respond to strain but their ERalpha content is regulated by estrogen. J. Bone Miner. Res. *21*, 1297–1306.

Accession Numbers

Microarray can be seen in Gene Expression Omnibus under accession number GSE7798.

ELSEVIER

Bone 40 (2007) 876–887

BONE

www.elsevier.com/locate/bone

Effects of aromatase inhibitors on human osteoblast and osteoblast-like cells: A possible androgenic bone protective effects induced by exemestane

Yasuhiro Miki [a], Takashi Suzuki [a], Masahito Hatori [b], Katsuhide Igarashi [c], Ken-ich Aisaki [c], Jun Kanno [c], Yasuhiro Nakamura [a], Miwa Uzuki [d], Takashi Sawai [c], Hironobu Sasano [a,*]

[a] *Department of Pathology, Tohoku University Graduate School of Medicine, 2-1 Seiryo-machi, Aoba-ku, Sendai, Miyagi, 980-8575, Japan*
[b] *Department of Orthopedic Surgery, Tohoku University Graduate School of Medicine, Sendai, Japan*
[c] *Division of Toxicology, National Institute of Health Sciences, Biological Safety Research Center, Setagaya, Tokyo, Japan*
[d] *Department of Pathology, Iwate Medical College, Morioka, Japan*

Received 21 April 2006; revised 6 November 2006; accepted 14 November 2006
Available online 28 December 2006

Abstract

Effects of aromatase inhibitors (AIs) on the human skeletal system due to systemic estrogen depletion are becoming clinically important due to their increasing use as an adjuvant therapy in postmenopausal women with breast cancer. However, possible effects of AIs on human bone cells have remained largely unknown. We therefore studied effects of AIs including the steroidal AI, exemestane (EXE), and non-steroidal AIs, Aromatase Inhibitor I (AI-I) and aminoglutethimide (AGM), on a human osteoblast. We employed a human osteoblast cell line, hFOB, which maintains relatively physiological status of estrogen and androgen pathways of human osteoblasts, i.e., expression of aromatase, androgen receptor (AR), and estrogen receptor (ER) β. We also employed osteoblast-like cell lines, Saos-2 and MG-63 which expressed aromatase, AR, and ERα/β in order to further evaluate the mechanisms of effects of AIs on osteoblasts. There was a significant increment in the number of the cells following 72 h treatment with EXE in hFOB and Saos-2 but not in MG-63, in which the level of AR mRNA was lower than that in hFOB and Saos-2. Alkaline phosphatase activity was also increased by EXE treatment in hFOB and Saos-2. Pretreatment with the AR blocker, flutamide, partially inhibited the effect of EXE. AI-I exerted no effects on osteoblast cell proliferation and AGM diminished the number of the cells. hFOB converted androstenedione into E2 and testosterone (TST). Both EXE and AI-I decreased E2 level and increased TST level. In a microarray analysis, gene profile patterns following treatment with EXE demonstrated similar patterns as with DHT but not with E2 treatment. The genes induced by EXE treatment were related to cell proliferation, differentiation which includes genes encoding cytoskeleton proteins. We also examined the expression levels of these genes using quantitative RT-PCR in hFOB and Saos-2 treated with EXE and DHT and with/without flutamide. HOXD11 gene known as bone morphogenesis factor and osteoblast growth-related genes were induced by EXE treatment as well as DHT treatment in both hFOB and Saos-2. These results indicated that the steroidal aromatase inhibitor, EXE, stimulated hFOB cell proliferation via both AR dependent and independent pathways.

Keywords: Osteoblast; Aromatase inhibitor; Androgen; Estrogen; Exemestane

Introduction

Results in various epidemiological or clinical studies demonstrated that estrogens play important protective roles in human skeletal as well as cardiovascular systems, and estrogen deficiency resulted in accelerating the development of osteoporosis in postmenopausal women [1–3]. In breast cancer of postmenopausal women, hormone therapies without any clinically deleterious effects due to estrogen deficiency on bone metabolism as well as lipid metabolisms are preferable. Estrogen deficiency has been generally detected in the patients with breast cancer following chemotherapy induced ovarian failure, gonadotropin analogue, and aromatase inhibitors (AIs) therapy [4]. Aromatase is the pivotal enzyme of *in situ* or intratumoral estrogen biosynthesis in postmenopausal breast cancer patients, and catalyzes the conversion from androgens into estrogens (Fig. 1A). AIs therefore play an important role in

* Corresponding author. Fax: +81 22 273 5976.
E-mail address: hsasano@patholo2.med.tohoku.ac.jp (H. Sasano).

8756-3282/$ - see front matter © 2006 Elsevier Inc. All rights reserved.
doi:10.1016/j.bone.2006.11.029

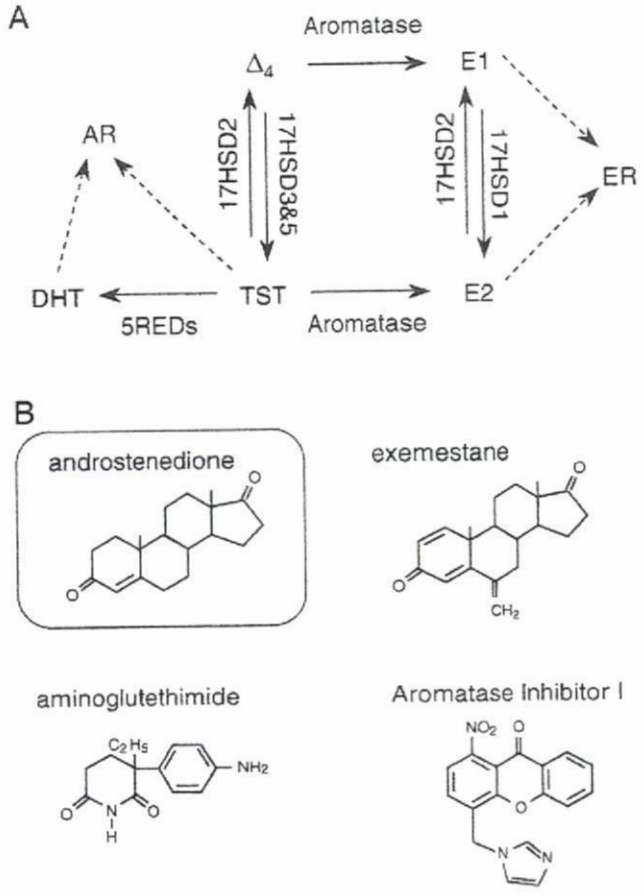

Fig. 1. (A) Summary of the pathway of estrogens and androgens production. Aromatase catalyzes the change from androstenedione (Δ4) and testosterone (TST) into estrone (E1) and estradiol (E2), respectively. 17HSD, 17β-hydroxysteroid dehydrogenase; 5REDs, 5α-reductase types 1 and 2; AR, androgen receptor; DHT, 5α-dihydrotestosterone; ER, estrogen receptor. (B) Structure of aromatase inhibitors used in this study. Androstenedione is a natural substrate of aromatase. Steroidal aromatase inhibitor, exemestane has an androstenedione-like structure.

clinical management of both primary and advanced breast cancer in postmenopausal women [5]. AIs are classified into two classes according to their modes of action. Type I AIs are steroidal inhibitions and one of them, exemestane (EXE) inhibits aromatase irreversibly and has an androstenedione (Δ_4)-like structure (Fig. 1B) [5–7]. Type II AIs are non-steroidal inhibitions and include aminoglutethimide (AGM), anastrozole, and letrozole [5].

Results of *in vivo* study using ovariectomized (OVX) rats demonstrated that EXE and its principal metabolite form, 17-hydroexemestane (17H-EXE) but not letrozole significantly prevented bone loss in OVX rats [8,9]. EXE and its principal metabolite, 17H-EXE, are structurally related to Δ_4 and bind to androgen receptor (AR) with relatively low affinity compared to 5α-dihydrotestosterone (DHT) [7]. These finding suggest that EXE may demonstrate protective effects toward bone tissues through its androgenic actions. However, detailed mechanisms of effects of EXE or androgen itself on human bone cells have remained largely unknown.

Various studies using human or animal bone tissues [10,11] and osteoblast cell culture using osteosarcoma cells [12,13] demonstrated that aromatase mRNA or protein was detected in osteoblast cells, which play an important role in bone remodeling. Therefore, in this study, we focused on effects of EXE in human osteoblast in an initial attempt to evaluate the effects of these AIs (summarized in Table 1 and Fig. 1B) [5–7,14], including AGM, EXE, and an experimental compound for inhibition of aromatase, Aromatase Inhibitor I (AI-I) [14] on human osteoblast and osteoblast-like cell lines. In our present study, we employed normal human cell line, hFOB, which maintains native characteristics of sex steroid hormone pathway of human osteoblasts, i.e., expression of AR, ERβ but not ERα, and aromatase. We also employed other osteoblast-like cell lines, Saos-2 and MG-63 which expressed ERα as well as ERβ in order to further study the mechanisms of effects of AI on human osteoblasts. We first examined the effects of estradiol (E2), DHT, progesterone (Prg), and AIs described above on cell proliferation of these cell lines, because the status of cell proliferation is important in the maintenance of homeostasis of bone tissue [15]. In addition, the effects of AIs on the conversion ratio of Δ_4 into E2 or testosterone (TST) in hFOB cultured medium were examined. We then screened E2, DHT, and EXE responsive genes using a microarray analysis in these cells, in order to further characterize the possible genomic effects of EXE on cell proliferation of osteoblasts. In this microarray analysis, hFOB was employed in order to examine the effects of E2, DHT, and EXE on native status of human osteoblasts but not on pathological status of osteoblasts such as osteosarcomas.

Materials and methods

Chemicals

Exemestane (EXE; FCE24304; 6-methyleneandrosta-1,4-diene-3,17-dione) and 17-hydroexemestane (17H-EXE; FCE25071; 6-methyleneandrosta-1,4-diene-17β-ol-3-one) were obtained from Pfizer, Inc. (MI, USA). Aminoglutethimide (AGM) and Aromatase Inhibitor I [AI-I; 4-(Imidazolylmethyl)-1-nitro-9*H*-9-xanthenone] were obtained from Sigma-Aldrich Co. (MO, USA) and EMD Biosciences, Inc. (CA, USA), respectively. Estradiol (E2), progesterone (Prg), and RU38,486 (RU; mifepristone), spironolactone were obtained from Sigma-Aldrich. ICI 182,780 (ICI; fulvestrant) and hydroxyflutamide (OHF) were obtained from Tocris Cookson Inc. (MO, USA) and Toronto Research Chemicals, Inc. (Ontario, Canada), respectively. 5α-dihydrotestosterone (DHT) was obtained from Wako Pure Chemical industries, Ltd. (Osaka, Japan).

Table 1
Aromatase inhibitors used in this study

	Aminoglutethimide	Exemestane	Aromatase inhibitor I
Trademark [a]	Cytadren®	Aromasin®	–
Type [b]	Type II	Type I	Type II
Generation	First	Third	–
IC50 (nM) [c]	3000	50	40

[a] Cytadren® is trademark of Novartis Pharmaseutical Corporation. Aromasin® is trademark of Pfizer Inc. Aromatase Inhibitor I is non-clinical compound o Calbiochem®.

[b] Type I is steroidal compound. Type II is a non-steroidal compound.

[c] Refs, Aminoglutethimide and Exemestane are Miller et al. [5]; Aromatas Inhibitor I is Recanatini et al. [14].

These materials were dissolved in pure ethanol (Wako Pure Chemical industries) and serially diluted (final concentrations: 10^{-12} M to 10^{-5} M), respectively. AGM was dissolved in DMSO (Wako Pure Chemical industries). The final concentration of ethanol and DMSO used in this study did not exceed 0.05%.

Osteoblast cell and osteoblast-like cell lines and culture conditions

Human normal osteoblast cell, hFOB 1.19 cell line (CRL-11372) was obtained from American Type Culture Collection (VA, USA). hFOB 1.19 cell was cultured according to the protocol previously described [16]. The cell line was maintained in a mixture of Dulbecco's Modified Eagle Medium and Ham's F12 medium (1:1) without phenol red (Invitrogen Corporation, CA, USA) supplemented with 10% fetal bovine serum (FBS; JRH Biosciences, KS, USA) and 50 mg/mL G 418 sulfate (EMD Biosciences). Human osteosarcoma cell lines Saos-2 and MG-63 were provided from the Cell Resource Center for Biomedical Research, Tohoku University (Sendai, Japan) and were maintained in a RPMI-1640 (Sigma-Aldrich) with 10% FBS. These cells were pre-incubated for 24 h with FBS-free medium prior to examination in order to remove exo-/endogenous steroid hormones from the culture medium and study the effects of various compounds in the absence of steroids and also to synchronize the cell cycle. Different concentrations of test compounds were added, and the assay was terminated after 3 or 5 days by removing the medium from wells. Steroid blockers were added simultaneously.

Characteristics of hFOB, Saos-2, and MG-63

Expressions of relevant steroid receptors, i.e., ERα, ERβ, and AR were determined using quantitative RT-PCR methods in hFOB, Saos-2, and MG-63 cell lines. mRNA transcripts of steroid synthesis/metabolite enzymes, aromatase, 17β-hydroxysteroid dehydrogenase (17β-HSD) types 1, 2, 3, 4, and 5, and 5α-reductase (5α-Red) types 1 and 2 were all evaluated using RT-PCR methods. The details of quantitative RT-PCR including primer sets employed were previously described in detail [17,18]. Positive controls for these receptors and enzymes were cell lines of human breast cancer, T-47D, and human prostate cancer, LNCaP obtained from Cell Resource Center for Biomedical Research, Tohoku University (Sendai, Japan). Alkaline phosphatase (ALP), an osteoblast-specific marker, was also studied using RT-PCR for characterization of these cell lines.

Estradiol and testosterone production assay

hFOB cells were plated in 10 mm dishes at a density of 10^6 viable cells and cultured for 48 h. Then media were changed to FBS-free medium, and hFOB cells were incubated with 10^{-7} M androstenedione (Δ_4; Sigma-Aldrich) in the presence or absence of EXE or AI-I (10^{-7} M). The media were then collected after 24 h, and E2 and TST were measured by solid-phase radioimmunoassay. Radioimmunoassay was performed in SRL Inc. (Tokyo, Japan) using DPC estradiol kit and DPC total testosterone kit (Diagnostic Products Corporation, LA, USA). In addition, we confirmed that the concentrations of E2 and TST were under the detection limits (E2, 5 pg/mL; TST, 30 pg/mL) in the serum- and phenol red-free medium.

Cell proliferation assay

hFOB, Saos-2, and MG-63 cells were treated with steroids and test compounds for 24, 48, and 72 h, when specimens were harvested and evaluated for cell proliferation using the WST-8 method (Cell Counting Kit-8; Dojindo Inc., Kumamoto, Japan) [18]. Optical densities (OD, 450 nm) were evaluated using a SpectraMax 190 microplate reader (Molecular Devices, Corp., CA, USA) and Softmax Pro 4.3 microplate analysis software (Molecular Devices). The status of proliferation (%) was calculated according to the following equation: (cell OD value after test materials treated / vehicle control cell OD value) × 100.

Alkaline phosphatase activity assay

hFOB, Saos-2, and MG-63 cells were plated in 48 well plate at a density of 10^6 viable cells and cultured for 48 h. All cell lines were treated with 10^{-9} to 10^{-7} M exemestane for 72 h, when cells were lysed with 0.05% Triton X-100 (Wako Pure Chemical industries) and evaluated for alkaline phosphatase activity

Table 2
Primer sequences used in quantitative RT-PCR analysis

cDNA	GB#	Sequence	cDNA position	Size (bp)
MYBL2	NM_002466	Forward 5′-GTAACAGCCTCACGCCCAAGA-3′ Reverse 5′-TCCAATGTGTCCTGTTTGTTCCA-3′	1522–1615	94
OSTM1	NM_014028	Forward 5′-TTGAGAATAAGGCTGAACCTGGAAC-3′ Reverse 5′-TTACAGGCACTGTGTCACTGCAAG-3′	801–926	126
HOXD11[a]	NM_021192	Forward 5′-CAC TGT CCT TGG GTT TAA TG-3′ Reverse 5′-GGT AAA ATT GTA ACG GGA CG-3′	1091–1245	174
GPC2	NM_152742	Forward 5′-AGA AAT GTG GTC AGC GAA GC-3′ Reverse 5′-ACA CCT TCG CAC TGT TTT CC-3′	871-1183	313
ADCYAP1R1	NM_001118	Forward 5′-CAG CAA AAG GGA AAG ACT CG-3′ Reverse 5′-GAG CTG CTC TTG CTC AGG AT-3′	1351–1584	234
COL1A1	NM_000088	Forward 5′-GGT GGT GGT TAT GAC TTT GGT T-3′ Reverse 5′-CTT GGC TGG GAT GTT TTC AGG T-3′	3784–4092	309
SMAD1[a]	NM_005900	Forward 5′-GGT TCA CCT CAT AAT CCT-3′ Reverse 5′-CCT TTG TCA GTT CTC AAT C-3′	1779–1887	127
SMAD5[a]	NM_005903	Forward 5′-AGC TAA AGC CGT TGG ATA-3′ Reverse 5′-AGG CAC TAA TAC TGG AGG T-3′	668–768	119
RUNX2	NM_004348	Forward 5′-GTG GAC GAG GCA AGA GTT T-3′ Reverse 5′-TAC TGG GAT GAG GAA TGC G-3′	782–961	198
SPARC	NM_003118	Forward 5′-CCT GTA CAC TGG CAG TTC-3′ Reverse 5′-CCA GGG CGA TGT ACT TGT C-3′	793–937	163
ALP	NM_000478	Forward 5′-ACC ATT CCC ACG TCT TCA CA-3′ Reverse 5′-AGA CAT TCT CTC GTT CAC CGC C-3′	1379–1540	162
RPL13A	NM_012423	Forward 5′-CCT GGA GGA GAA GAG GAA AGA GA-3′ Reverse 5′-TTG AGG ACC TCT GTG TAT TTG TCA A-3′	487–612	126

GB#, GeneBank accession number.
All primer sets were designed using OLIGO Primer Analysis Software (TAKARA Bio Inc., Shiga, Japan).
[a] Forward and reverse primers were located in sama exon.

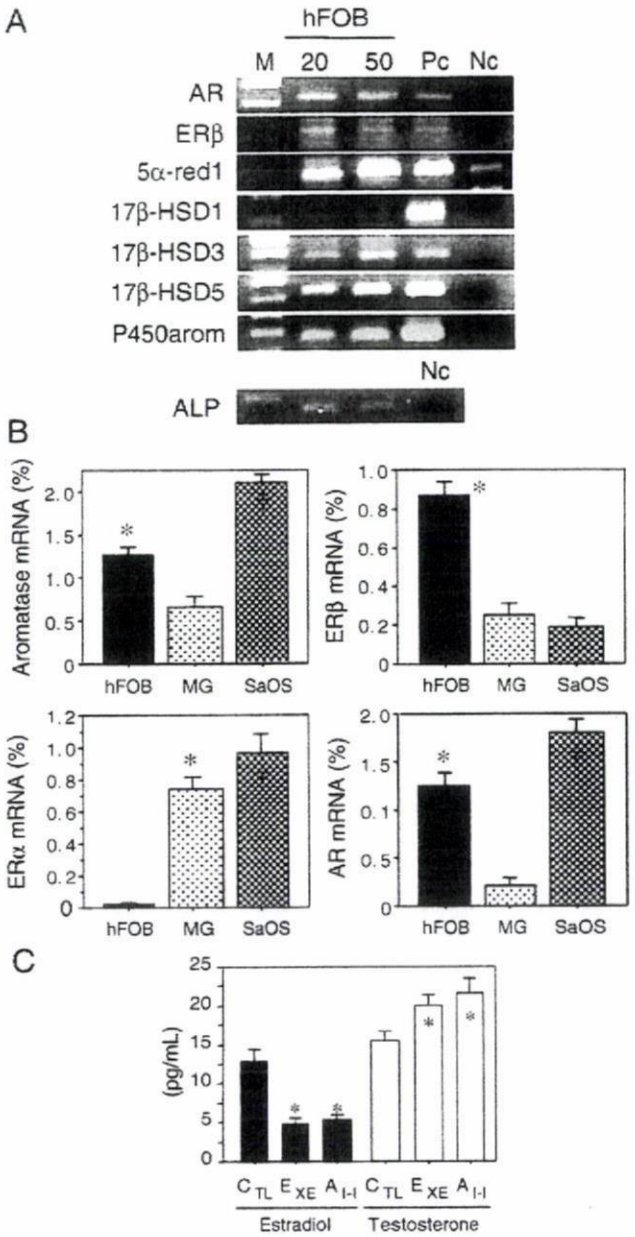

Fig. 2. (A) Results of RT-PCR analysis of steroid hormone receptors and steroid-related enzymes. Both 20 and 50 ng/μL cDNA of hFOB were used for PCR (ALP was 20 ng/μL alone). AR, androgen receptor; ER, estrogen receptor; 5α-red1, 5α-reductase type 1; 17β-HSD, 17β-hydroxysteroid dehydrogenase; P450 arom, aromatase; M, molecular marker; Pc, positive control; Nc, negative control. (B) Expression levels of aromatase, AR, ERα, and ERβ in hFOB, Saos-2, and MG-63. *$p<0.05$ vs. MG-63 (aromatase and AR), vs. MG-63 and vs. Saos-2 (ERβ), vs. hFOB (ERα); †$p<0.05$ vs. hFOB and MG-63 (aromatase and AR), vs. MG-63 and hFOB (ERα). (C) Estradiol and testosterone productions in hFOB cells. The data are expressed as the mean SD ($n=3$). *$p<0.05$ vs. control cells (CTL). EXE, 10^{-7} M exemestane; AI-I, 10^{-7} M aromatase inhibitor I.

using the *p*-nitrophenylphosphate method (LabAssay ALP; Wako Pure Chemical industries) [19]. Optical densities (OD, 405 nm) were evaluated using a SpectraMax 190 microplate reader (Molecular Devices) and Softmax Pro 4.3 microplate analysis software (Molecular Devices). ALP activity (units/μL)=(concentration of *p*-nitrophenol/15 min)×1 (dilution factor of sample). The ALP activities were presented as units/μL/10^6 cells. The ALP activity levels in each case were represented as a ratio of vehicle control (%).

Microarray analysis

The procedure was based on a previously reported study [20]. Cell lysates were prepared using RLT buffer (QIAGEN GmbH, Hilden, Germany). Total RNA was extracted using RNeasy Mini Kit (QIAGEN). First-strand cDNA was synthesized by incubating 5 μg of total RNA with 200 U SuperScript II reverse transcriptase (Invitrogen), 100 pmol T7-(dT)24 primer (Invitrogen). Ten units of T4 DNA polymerase (Invitrogen) were then added, and the dsDNA was mixed with T7 RNA polymerase (Invitrogen). The purified cRNA was fragmented at 300–500 bp as target solution. Hybridization was performed with the GeneChip Human Genome 133 ver. 2.0 (Affymetrix, Inc., CA, USA). The reacted arrays were then scanned as digital image files and scanned data were analyzed with GeneChip software (Affymetrix). Relative levels of gene expression were calculated by global normalization.

Data were subjected to hierarchical clustering analysis and visualization using the Cluster and TreeView programs (Stanford University) in order to generate tree structures based on the degree of similarity, as well as matrices comparing the levels of expression of individual genes in each sample [21].

Real-time PCR

Real-time PCR was carried out using the LightCycler System and the FastStart DNA Master SYBR Green I (Roche Diagnostics GmbH, Mannheim, Germany). The primer sequences used in this study are summarized in Table 2. An initial denaturing step of 95 °C for 10 min was followed by 35 cycles, respectively, at 95 °C for 10 min; 15 s annealing at 65 °C (ALP, COL1A1), 64 °C (MYBL2, OSTM1, RPL13A), 62 °C (SMAD1, SMAD5, SPARC, RUNX2), or 60 °C (HOXD11); and extension for 15 s at 72 °C. Negative control experiments included those lacking cDNA substrates to confirm the presence of exogenous contaminant DNA. No amplified products were detected under these conditions. The mRNA levels in each case were represented as a ratio of RPL13A (%) [22].

Immunohistochemistry of AR

Five non-pathological bone tissues were retrieved from surgical pathology files (two females and three males, 17 to 55 years old) of Department of Pathology, Tohoku University Hospital (Sendai, Japan).

Tissue sections were immunostained using a biotin-streptavidin method with Histofine kit (Nichirei Co. Ltd., Tokyo, Japan). The monoclonal antibody for AR (AR411) [23] was obtained from DakoCytomation (Kyoto, Japan). Experimental procedures employed in our present study have been previously described in detail [22,23]. The dilutions of primary AR antibody were 1:100. The antigen-antibody complex was then visualized with 3,3′-diaminobenzidine solution, and counterstained with hematoxylin. Prostate cancer was used as a positive control for AR. Normal mouse IgG was used as a negative control for immunostaining and no specific immunoreactivity was detected.

Statistical analysis

Results were expressed as mean±SD. Statistical analysis was performed with the StatView 5.0 J software (SAS Institute Inc., NC, USA). All data were analyzed by analysis of variance (ANOVA) followed by post hoc Bonferroni/Dunnett multiple comparison test. A p-value<0.05 was considered to indicate statistical significance.

Results

Characteristics of hFOB, MG-63, and Saos-2 cell line

Characteristics of osteoblast and osteoblast-like cell lines are summarized in Figs. 2A and B. hFOB cells expressed mRNA transcripts of AR and ERβ. Relatively low level of ERα mRNA transcript was detected in hFOB cells. Aromatase, 17β-HSD type 1, 3, and 5, and 5α-Red types 1 and 2 mRNA transcripts were all detected in hFOB cells by

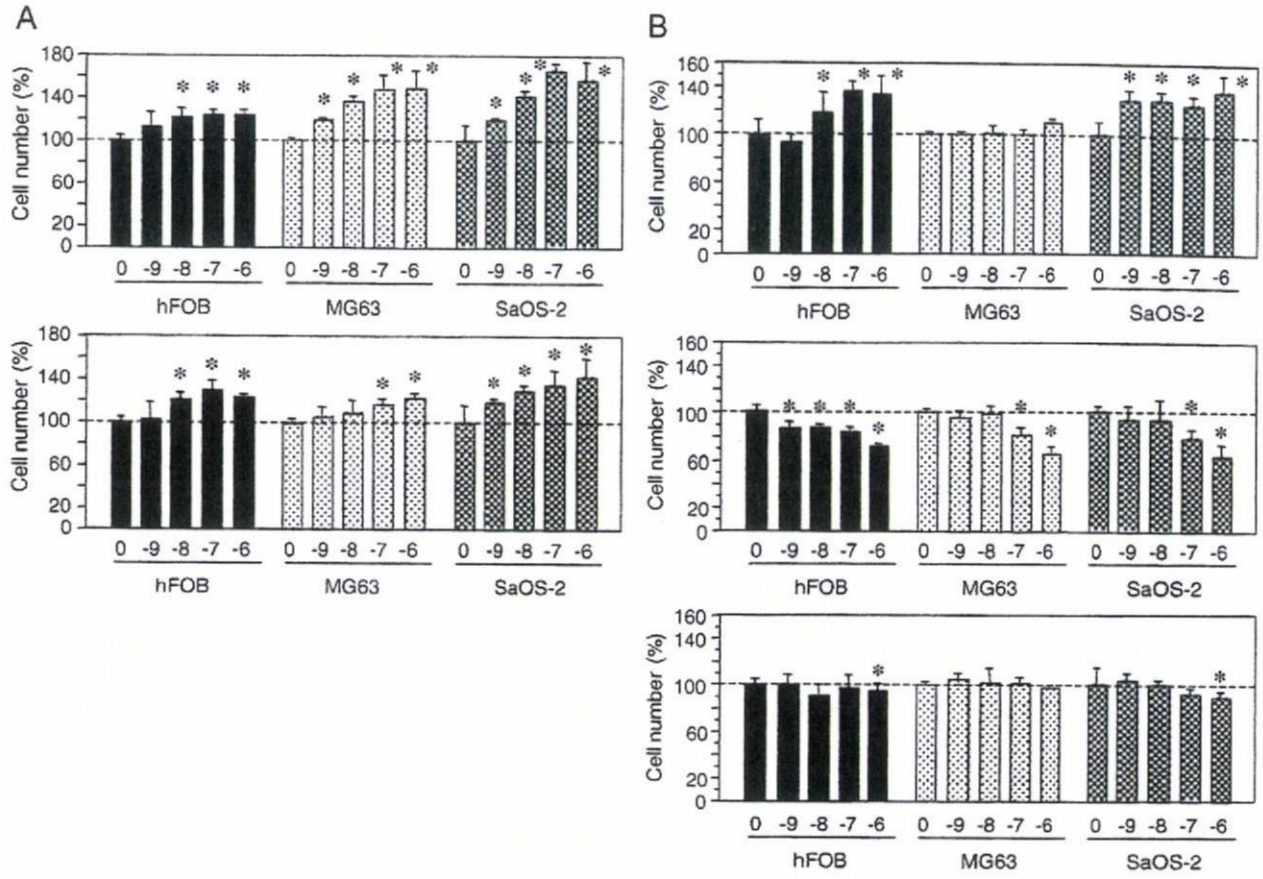

Fig. 3. (A) Proliferation of hFOB cells treated by estradiol (top) and 5α-DHT (bottom). *$p<0.05$ vs. vehicle control (0). (B) Proliferation of hFOB cells treated by exemestane (top), aminogluthetimide (middle), and Aromatase Inhibitor-I (bottom). *$p<0.05$ vs. vehicle control (0). $n=5$.

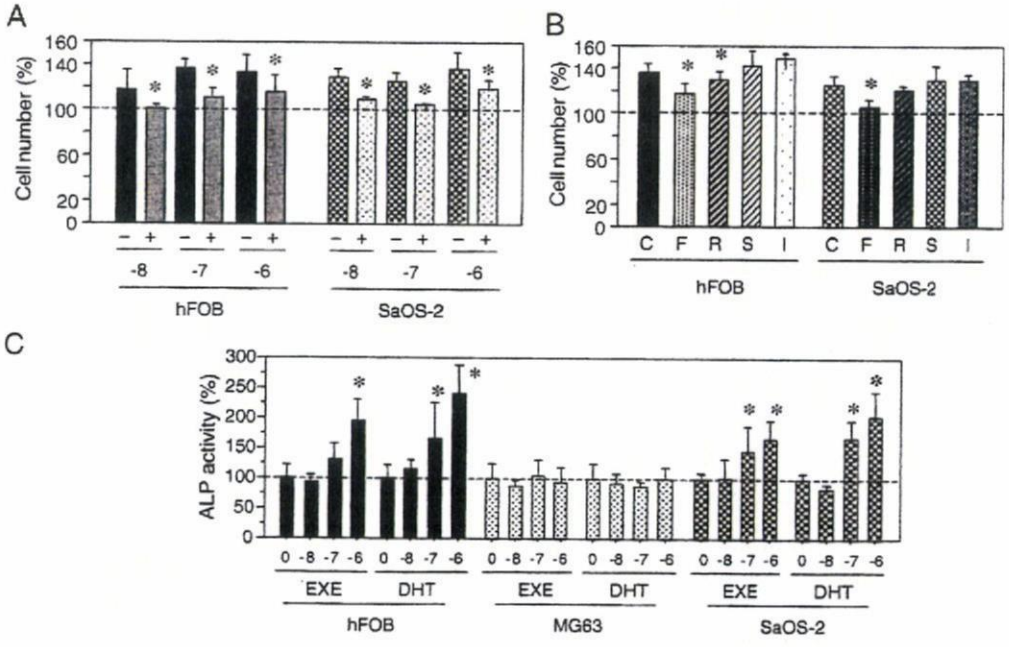

Fig. 4. (A) Effects of hydroxyflutamide on exemestane (10^{-8} to 10^{-6} M) stimulated the cell proliferation of both hFOB and Saos-2. With (+) or without (−) hydroxyflutamide, $p<0.05$ vs. without hydroxyflutamide (*). (B) Effects of steroid receptor blockers on exemestane (10^{-7} M) stimulated cell proliferation of hFOB and Saos-2. C, 10^{-7} M exemestane; F, hydroxyflutamide (5×10^{-6} M); R, RU38,486 (5×10^{-6} M); S, spironolactone (5×10^{-6} M); I, ICI182,720 (5×10^{-6} M). *$p<0.05$ vs. C (C) ALP activity in hFOB, Saos-2, MG-63 treated with exemestane (EXE, 10^{-8} to 10^{-6} M), or 5α-DHT (DHT, 10^{-8} to 10^{-6} M). *$p<0.05$ vs. vehicle control (0).

RT-PCR. Aromatase, ERα, ERβ, and AR were all detected in osteoblast-like cell lines, Saos-2 and MG-63 (Fig. 2B). In hFOB cell, expression of ERβ mRNA was more predominant than that of ERα mRNA. ERα mRNA as well as ERβ mRNA was detected in Saos-2 and MG-63 cells. The levels of AR mRNA expression in both hFOB and Saos-2 were significantly higher ($p=0.01$) than that in MG-63. ALP mRNA was also detected in intact hFOB, Saos-2, and MG-63 cells (data not present), respectively.

Estradiol and testosterone production

Results were summarized in Fig. 2C. The E2 levels in the medium of hFOB supplemented with Δ_4 treated with EXE or AI-I were significantly lower than that of cells without AIs. The levels of TST in the medium of hFOB supplemented with Δ4 treated with EXE or AI-I were significantly higher than that of cells without AIs.

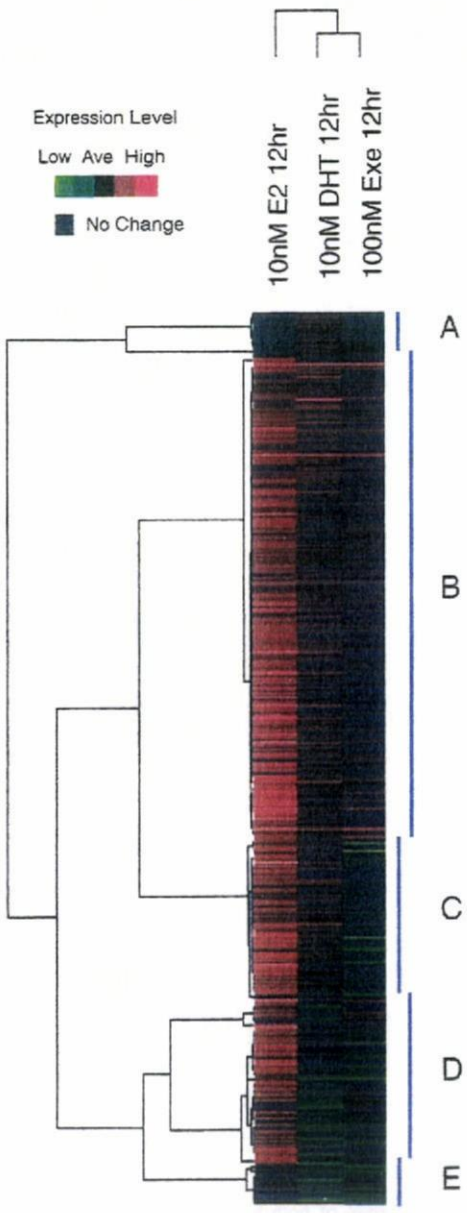

Fig. 5. In clustering analysis of the expression levels of each gene in hFOB cells treated with estradiol (E2), 5α-dihydrotestosterone (DHT), and exemestane (Exe).

Cell proliferation

Results of the cell proliferation assays are summarized in Figs. 3 and 4. There was a significant increment in the number of the cells after 72 h in hFOB, Saos-2, and MG-63 cells treated with 10^{-9} M (Saos-2 and MG-63) or 10^{-8} M (hFOB) to 10^{-6} M E2 (Fig. 3A). The cell number of hFOB and Saos-2 cells treated by 10^{-9} M (Saos-2) or 10^{-8} M (hFOB) to 10^{-6} DHT for 72 h was also significantly higher than control (Fig. 3A). The number of MG-63 cells was significantly increased only by high dose of DHT (10^{-7} M and 10^{-6} M) treatments (Fig. 3A). Prg (10^{-9} M to 10^{-6} M) treatments did not change the number of cells even after 72 h in all three cell lines examined (data not present).

Both EXE (Fig. 3B) and 17H-EXE (data not present) treatments of 10^{-8} M to 10^{-6} M, which were comparable to pharmacological inhibition doses of aromatization (Table 1), significantly increased the hFOB cell number for 72 h, respectively. In Saos-2 cells treated with relatively low dose, 10^{-9} to 10^{-6} M EXE, there was a significant increment in the number of the cells after 72 h (Fig. 3B). However, all the dose (10^{-9} M to 10^{-6} M) of EXE employed did not results in the change of cell number of MG-63 even after 72 h of treatment (Fig. 3B). The cell number of both hFOB and Saos-2 cells treated by both 10^{-6} M EXE and/or 17H-EXE for 48 h was also significantly higher than that treated for 24 h (data not present).

AGM treatment [10^{-9} (hFOB) or 10^{-7} (Saos-2 and MG-63) to 10^{-6} M] diminished the number of these three cells (Fig. 3B) and morphological changes in these cells were consistent with those caused by cytotoxic effects (data not present). AI-I treatment (10^{-9} to 10^{-7} M) was not associated with significant increment of the cell number in these cell lines (Fig. 3B). Only high dose (10^{-6} M) of AI-I significantly diminished the cell numbers of hFOB and Saos-2 but not of MG-63 (Fig. 3B).

The androgen receptor antagonist OHF (5×10^{-6} M) diminished the effects of EXE on these increments of both hFOB and Saos-2 cells (Figs. 4A and B). Treatment with RU but not spironolactone and ICI also inhibited EXE effects on hFOB cells (Fig. 4B).

ALP activity assay

Results of the ALP activity assay were summarized in Fig. 4C. There was a significant increment in the ALP activity of both hFOB and Saos-2 cells treated with 10^{-7} M (Saos-2) and/or 10^{-6} M (hFOB and Saos-2) EXE. Both 10^{-7} M and 10^{-6} M DHT treatment also increased the ALP activity in hFOB and Saos-2 cells, respectively. There were no changes of ALP activity in MG-63 treated with 10^{-8} M to 10^{-6} M of EXE and DHT, respectively.

Table 3a
Genes induced by exemestane treatment in hFOB cells—2.0 higher

	Gene title	Gene symbol	Raw data			Ratio	
			C	D	Ex	D	Ex
NM_002466	V-myb myeloblastosis viral oncogene homolog (avian)-like 2	**MYBL2**	70.9	156.9	150.3	2.2	2.1
AW444985	–	–	57.8	124.7	127.1	2.2	2.2
AF143684	Myosin IXB	MYO9B	48.3	64.4	122.2	1.3	2.5
NM_024682	TBC1 domain family, member 17	TBC1D17	31.7	37.6	64.8	1.2	2.0
BE965311	Chromosome 16 open reading frame 23	C16orf23	29.2	44.2	64.0	1.5	2.2
NM_004233	CD83 antigen (activated B lymphocytes, immunoglobulin superfamily)	CD83	29.0	66.5	60.9	2.3	2.1
AI806031	Skeletal muscle and kidney enriched inositol phosphatase	SKIP	27.7	48.6	55.4	1.8	2.0
AL136729	Ring finger protein 123	RNF123	20.0	23.7	41.3	1.2	2.1
NM_015254	Kinesin family member 13B	KIF13B	13.0	24.5	39.4	1.9	3.0
AL110249	Chromosome 20 open reading frame 194	C20orf194	13.4	39.0	29.7	2.9	2.2
AF208502	Early B-cell factor	EBF	12.5	21.1	28.5	1.7	2.3
AW007221	Solute carrier family 13 (sodium/sulfate symporters), member 4	SLC13A4	12.3	9.6	27.8	0.8	2.3
AB007458	TP53 activated protein 1	TP53AP1	12.6	22.2	26.2	1.8	2.1
AV713913	Osteopetrosis associated transmembrane protein 1	**OSTM1**	9.8	16.5	21.3	1.7	2.2
BF339201	THAP domain containing 6	THAP6	6.0	14.0	20.6	2.3	3.4
AK000455	Hypothetical gene MGC16733 similar to CG12113	MGC16733	7.3	16.6	18.8	2.3	2.6
AW974816	–	–	2.2	16.0	17.2	7.2	7.7
AK025325	Transcribed locus, moderately similar to NP_689573.2 zinc finger protein 573	–	7.3	11.4	16.2	1.6	2.2
NM_021192	Homeo box D11	**HOXD11**	5.3	16.2	15.8	3.0	3.0
NM_022169	ATP-binding cassette, sub-family G (WHITE), member 4	ABCG4	7.0	10.5	15.7	1.5	2.2
R62907	Disabled homolog 2, mitogen-responsive phosphoprotein (*Drosophila*)	DAB2	7.7	13.0	15.5	1.7	2.0
NM_002661	Phospholipase C, gamma 2 (phosphatidylinositol-specific)	PLCG2	7.3	12.3	15.3	1.7	2.1
BG393032	Solute carrier family 13 (sodium/sulfate symporters), member 4	SLC13A4	6.4	6.7	15.1	1.0	2.3
BC002794	Tumor necrosis factor receptor superfamily, member 14	TNFRSF14	6.2	11.3	13.6	1.8	2.2
BC042908	KIAA0690	KIAA0690	5.6	7.4	13.5	1.3	2.4
AW451961	Adenylate cyclase activating polypeptide 1 (pituitary) receptor type I	**ADCYAP1R1**	4.3	11.7	13.2	2.7	3.1
AI863264	Glypican 2 (cerebroglycan)	**GPC2**	5.3	7.2	13.2	1.3	2.5
AF130050	ACA47 scaRNA gene	-	5.6	9.5	12.9	1.7	2.3
AK022326	Hypothetical gene supported by AK022326	-	6.1	12.7	12.9	2.1	2.1
AK021807	Low density lipoprotein receptor-related protein 11	LRP11	5.9	6.2	12.8	1.0	2.2
AU155415	Kallikrein 7 (chymotryptic, stratum corneum)	KLK7	5.6	13.5	12.7	2.4	2.3
BF673779	Hypothetical protein FLJ30834	FLJ30834	5.5	6.3	12.3	1.1	2.2
AV646335	–	–	2.6	13.0	11.2	5.0	4.3
BC040600	–	–	5.0	5.4	10.6	1.1	2.1
AI131035	–	–	5.1	9.2	10.5	1.8	2.1

C, vehicle control; D, 5α-dihydrotestosterone; Ex, exemestane. Genes that performed quantitative RT-PCR were described in bold style.

Microarray/clustering analysis

In hFOB cells, the hierarchical clustering analysis contains 430 genes which demonstrated expression ratios above 2.0-fold and below 0.5-fold compared with vehicle control cells after 12 h of each gene treated with 10^{-8} M E2, 10^{-8} M DHT, or 10^{-7} M EXE. The expression profiles of EXE treated cells were closely related to those of DHT (Fig. 5). In this study, we focused on 35 genes (Table 3a), which were all up-regulated twice or more than control. In this group, we further focused on 5 genes, B-Myb 2 (MYBL2), osteopetrosis associated transmembrane protein 1 (OSTM1), homeo box D 11 (HOXD11), adenylate cyclase activating polypeptide 1 receptor (ADCYAP1R1), and glypican 2 (GPC2) which are all considered to play important roles in EXE or DHT induced cell proliferation. We therefore examined whether these 5 genes were increased by EXE or DHT treatments using quantitative RT-PCR in hFOB cells. We also examined the validation of results of microarray analysis obtained in hFOB cells in Saos-2 and MG-63 cells.

Validation of microarray analysis using quantitative RT-PCR

In hFOB cells, all of these 5 genes described above were significantly increased by 10^{-7} M EXE treatment, and 3/5 genes (except for OSTM1 and GPC2) were also significantly increased by 10^{-8} M DHT treatment. HOXD11 and ADCYAP1R1 genes increased by both EXE and DHT were significantly diminished by OHF (5×10^{-6} M) treatment (Figs. 6A–C).

The similar results of changes of MYBL2 expression were also obtained in both Saos-2 and MG-63 treated with EXE and DHT, respectively (Fig. 6A). In addition, the results of HOXD11 expression in hFOB were equivalent to those in Saos-2 but not in MG-63 treated with EXE and DHT (Fig. 6B). Other genes induced by treatment of EXE and DHT in hFOB such as OSTM1, GPC2, and ADCYAP1R1 were not changed in both Saos-2 and MG-63 cells treated with EXE and DHT, respectively (data not present). AI-I or AGM treatment did not increase all of these genes expression in hFOB (data not present).

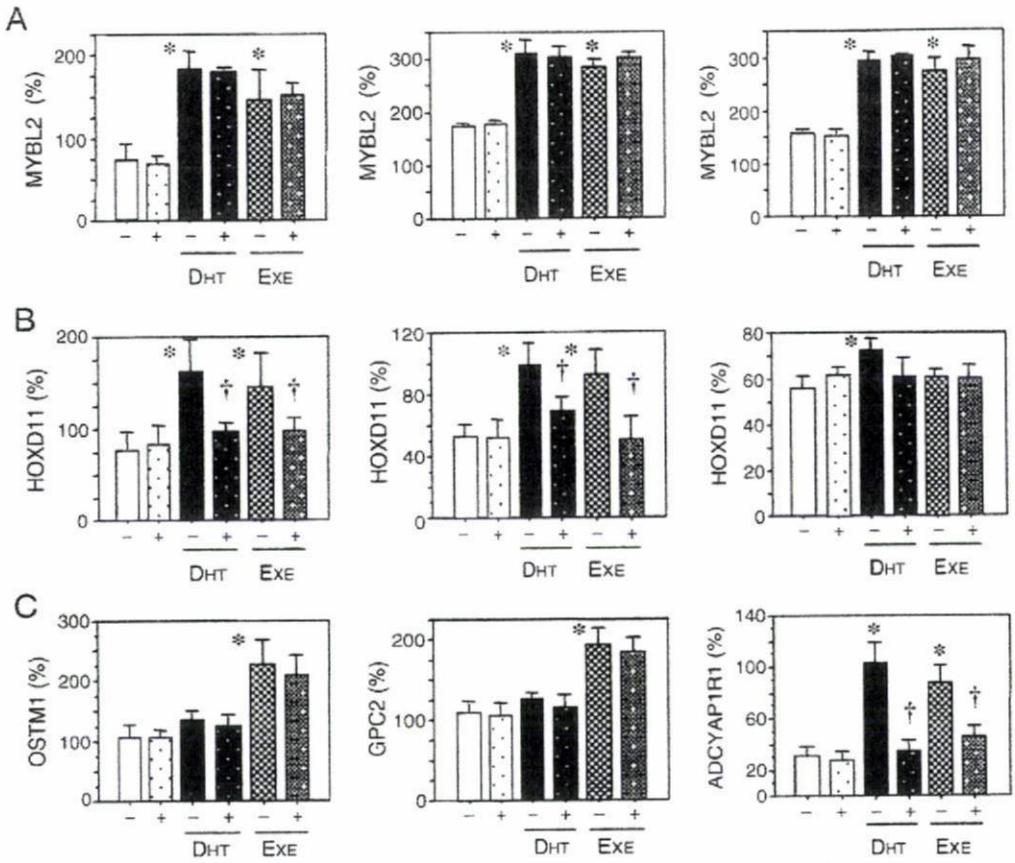

Fig. 6. Validation of microarray analysis. (A) Expression levels of MYBL2 in hFOB (left), Saos-2 (middle), and MG-63 (right). (B) Expression levels of HOXD11 in hFOB (left), Saos-2 (middle), and MG-63 (right). (C) Expression levels of OSTM1, GPC2, and ADCYAP1R1 in hFOB. DHT: 10^{-8} M 5α-dihydrotestosterone, EXE: 10^{-7} M Exemestane, with (+) or without (−) hydroxyflutamide, $p<0.05$ vs. control (*) or without hydroxyflutamide (†).

Analysis of osteoblast growth-related genes

Results of microarray analysis in hFOB cell demonstrated that osteoblast growth-related genes [24,25] such as COL1A1, SMAD1, SMAD5, SPARC, and RUNX2 were all up-regulated by exemestane (10^{-7} M) treatment but the degrees of increment were all under 2-fold (Table 3b). In this microarray analysis, other expression levels of previously reported osteoblast-related genes were not altered.

In hFOB cells, the validation analysis of these genes described above using quantitative RT-PCR (Fig. 7) demonstrated that 4/5 genes (except for COL1A1) were significantly increased by 10^{-7} M EXE treatment, and 4/5 genes (except for SMAD1) were also significantly increased by 10^{-8} M DHT treatment. The increased expression of the SMAD1, SMAD5, and SPARC genes by EXE or DHT, was significantly diminished by OHF (5×10^{-6} M) treatment. There were no effects of OHF pretreatment on the increased expression levels of RUNX2 that had occurred after both EXE and DHT treatments. Both AI-I and AGM treatment could not increase all of these genes expression in hFOB (data not present).

In Saos-2 cells, 4/5 genes (except for RUNX2) were significantly increased by 10^{-7} M EXE treatment, and 3/5 genes (except for RUNX2 and SMAD1) were also significantly increased by 10^{-8} M DHT treatment. The increment of the COL1A1, SMAD5, and SPARC genes expression by EXE or DHT, was significantly diminished by OHF (5×10^{-6} M) treatment. All of these 5 genes did not change in MG-63 cells treated with EXE or DHT, respectively (data not present).

Immunohistochemistry of AR

Marked AR immunoreactivity was detected in the nuclei of osteoblasts or lining cells but not in osteoclasts in four cases (Fig. 8). In these four cases, AR immunoreactivity was also detected in osteocytes and condrocytes. In one case, there was no immunoreactivity in all types of bone cells.

Discussion

In the clinical study of EXE compared to placebo administrated for two years [26,27], EXE modestly enhanced bone loss from the femoral neck without significant influence on lumber bone loss despite a marked systemic estrogen depletion. Furthermore, the risks of clinical bone fractures are considered to be lower with EXE treatment than that seen with non steroidal AIs [27,28], though it is also important to recognize that EXE has not been shown to significantly increase the amount of bone mass in various clinical studies of breast cancer patients [26,27]. The relative protective effect of EXE, a

Table 3b
Genes induced by exemestane treatment in hFOB cells—the osteoblast growth-related genes

	Gene title	Gene symbol	Raw data			Ratio	
			C	D	Ex	D	Ex
K01228	Collagen, type I, alpha 1	**COL1A1**	2797.2	3240.9	3058.5	1.2	1.1
BE221212	Collagen, type I, alpha 1	**COL1A1**	2741.1	3048.3	3052.2	1.1	1.1
AI743621	Collagen, type I, alpha 1	**COL1A1**	228.0	241.6	242.5	1.1	1.1
AA788711	Collagen, type I, alpha 2	COL1A2	2250.6	2474.3	2375.4	1.1	1.1
NM_000089	Collagen, type I, alpha 2	COL1A2	1749.1	1848.7	1787.6	1.1	1.0
M60485	Fibroblast growth factor receptor 1	FGFR1	178.9	185.7	198.6	1.0	1.1
BE467261	Fibroblast growth factor receptor 1	FGFR1	165.4	208.6	189.7	1.3	1.1
M63889	Fibroblast growth factor receptor 1	FGFR1	119.3	111.6	140.5	0.9	1.2
NM_023110	Fibroblast growth factor receptor 1	FGFR1	60.5	84.0	70.2	1.4	1.2
AU145411	Fibroblast growth factor receptor 1	FGFR1	29.2	44.1	37.5	1.5	1.3
AI359368	Fibroblast growth factor receptor 3	FGFR3	41.4	65.5	58.7	1.6	1.4
NM_001552	Insulin-like growth factor binding protein 4	IGFBP4	809.1	1027.5	1040.4	1.3	1.3
AL353944	Runt-related transcription factor 2	**RUNX2**	192.9	226.3	216.3	1.2	1.1
AU146891	SMAD, mothers against DPP homolog 1 (*Drosophila*)	**SMAD1**	161.2	195.6	204.6	1.2	1.3
NM_005901	SMAD, mothers against DPP homolog 2 (*Drosophila*)	SMAD2	100.3	108.2	113.7	1.1	1.1
NM_005902	SMAD, mothers against DPP homolog 3 (*Drosophila*)	SMAD3	110.2	106.5	127.7	1.0	1.2
BF526175	SMAD, mothers against DPP homolog 5 (*Drosophila*)	**SMAD5**	361.0	488.3	514.2	1.4	1.4
AI478523	SMAD, mothers against DPP homolog 5 (*Drosophila*)	SMAD5	300.7	384.9	346.9	1.3	1.2
AF010601	SMAD, mothers against DPP homolog 5 (*Drosophila*)	SMAD5	79.2	99.7	87.6	1.3	1.1
AY014180	SMAD-specific E3 ubiquitin protein ligase 2	SMURF2	804.2	844.7	851.8	1.1	1.1
AU157259	SMAD-specific E3 ubiquitin protein ligase 2	SMURF2	77.1	81.5	86.3	1.1	1.1
AL575922	Secreted protein, acidic, cysteine-rich (osteonectin)	**SPARC**	1702.1	1935.5	1925.8	1.1	1.1
BF508662	Sprouty homolog 1, antagonist of FGF signaling (*Drosophila*)	SPRY1	31.9	46.3	45.4	1.5	1.4
NM_014886	TGF beta-inducible nuclear protein 1	TINP1	1185.7	1259.5	1241.1	1.1	1.0

C, vehicle control; D, 5α-dihydrotestosterone; Ex, exemestane. Genes that performed quantitative RT-PCR were described in bold style.

steroidal aromatase inhibitor, has been therefore attributed to its actions through AR in osteoblasts. Systemic androgenic effects such as hypertricosis, hair loss, hoarseness, and acne have been reported only in 4% [6] of the patients treated with EXE (25 mg/day) and the frequency of these effects increases to approximately 10% in those treated with higher dose 200 mg/day of EXE [6]. This finding suggests that the patients treated with EXE are under relatively weak systemic androgenic effects. Androgen sensitivity has been well-known to be subject to great individual variation caused by AR gene CAG polymorphism in women as well as men [29,30]. Therefore, this 5 to 10% of the patients who manifested clinical androgenic effects by EXE treatment may be individuals associated with relatively enhanced androgenic sensitivity. Replacement therapy with TST is generally effective at restoring bone in hypogonadal men [31]. In female-to-male, genetic female transsexual subjects, high-dose TST therapy generally increased BMD at the femoral neck, despite decrement of E2 to postmenopausal levels [32,33]. Therefore, androgens may play an important role in bone protection in women as well as men.

The results of cell proliferation assay demonstrated that the cell number of MG-63 was increased by both E2 and DHT treatments, but the dose of DHT was relatively higher than that in two other cells. MG-63 expressed higher levels of ERα/β mRNA, but the level of AR mRNA was lower than that in both Saos-2 and hFOB. Both cell proliferation and ALP activity of MG-63 could not be stimulated by EXE treatment. Molecular mechanisms of androgen actions on osteoblasts have remained largely unknown. Androgen is well-known to stimulate osteoblast proliferation [34] and differentiation [35]. For instance, osteoprotegerin mRNA was increased by TST as well as DHT treatments in mouse 3T3-E1 cells [36].

AR and ERβ but not ERα are predominantly detected in osteoblasts located on human cancellous bone using immunohistochemical analysis [37]. Therefore, hFOB examined in this study is considered to maintain relatively native status of sex steroids pathways in human osteoblasts. Therefore, we employed hFOB for further examination of EXE effects on osteoblast gene expression pattern using microarray analysis. In this study, we demonstrated that the genes MYBL2 [38], OSTM1 [39], HOXD11 [40], ADCYAP1R1 [41], and GPC2 [42] were target genes of EXE alone or both EXE and DHT in hFOB using microarray/PCR analysis. These genes were demonstrated to be involved in regulation of cell cycle, differentiation, and transcription. In EXE or DHT treatment in hFOB and Saos-2, in which cells proliferations were stimulated, an increased expression of HOXD11 gene was detected. The product of the mouse Hoxd11 gene was reported to play a role in forelimb morphogenesis [40,43]. Therefore, these finding suggest that osteoblast cell proliferation stimulated by EXE treatment may depend on HOXD11 gene expression through AR. In this study, the cell proliferation of MG-63, which expressed relatively low level of AR, was not stimulated by EXE. In addition, HOXD11 gene expression was not up-regulated by EXE treatment in MG-63 cells. These results were also consist with the protective effects of EXE through potential androgen-HOXD11 pathway in osteoblast cells. In this study, we also examined the effects of EXE and DHT on osteoblast growth-related genes using micro-

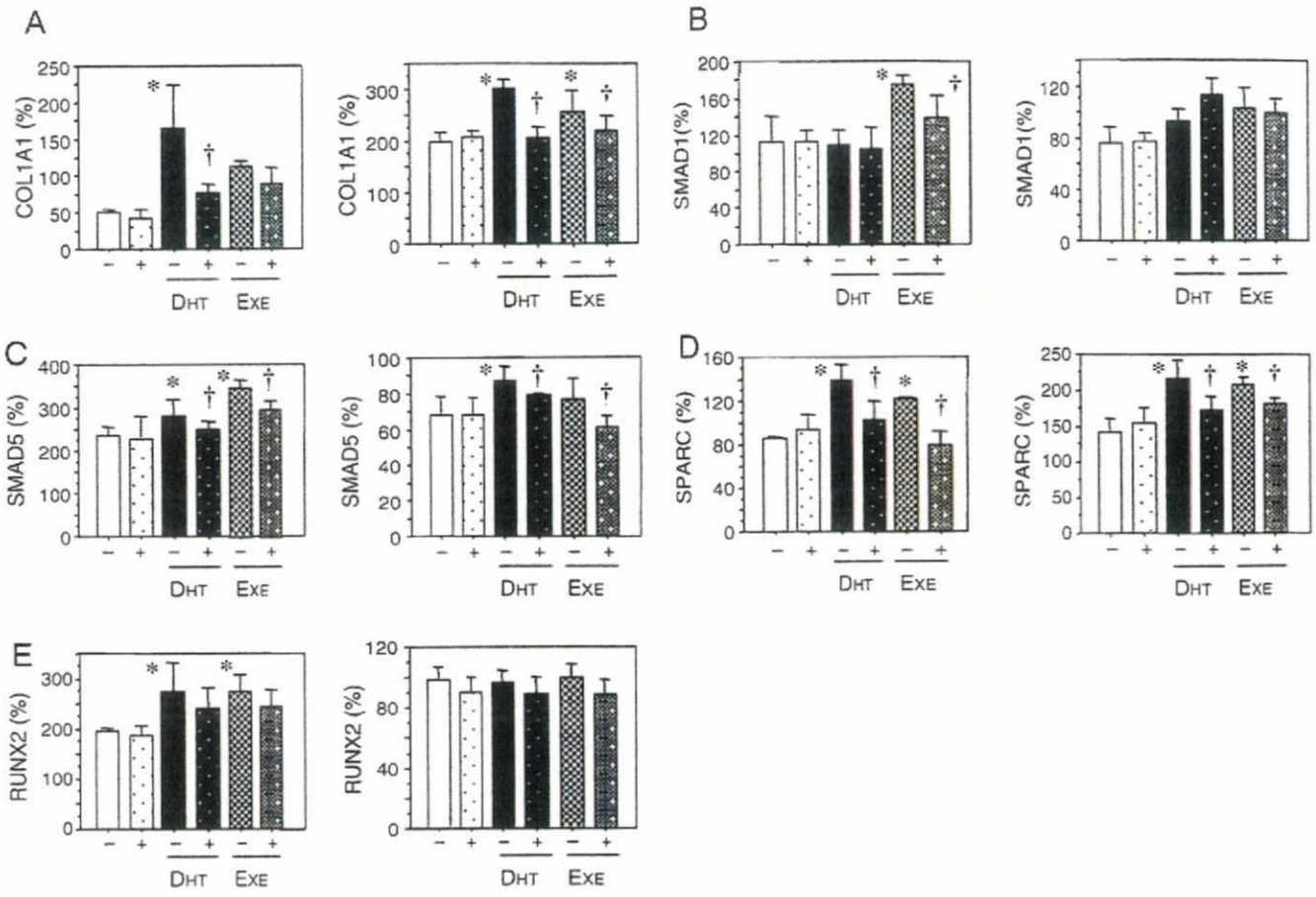

Fig. 7. Expression levels of osteoblast growth-related genes in hFOB (left) and Saos-2 (right). DHT: 10^{-8} M 5α-dihydrotestosterone, EXE: 10^{-7} M Exemestane, with (+) or without (−) hydroxyflutamide, $p<0.05$ vs. control (*) or without hydroxyflutamide (†).

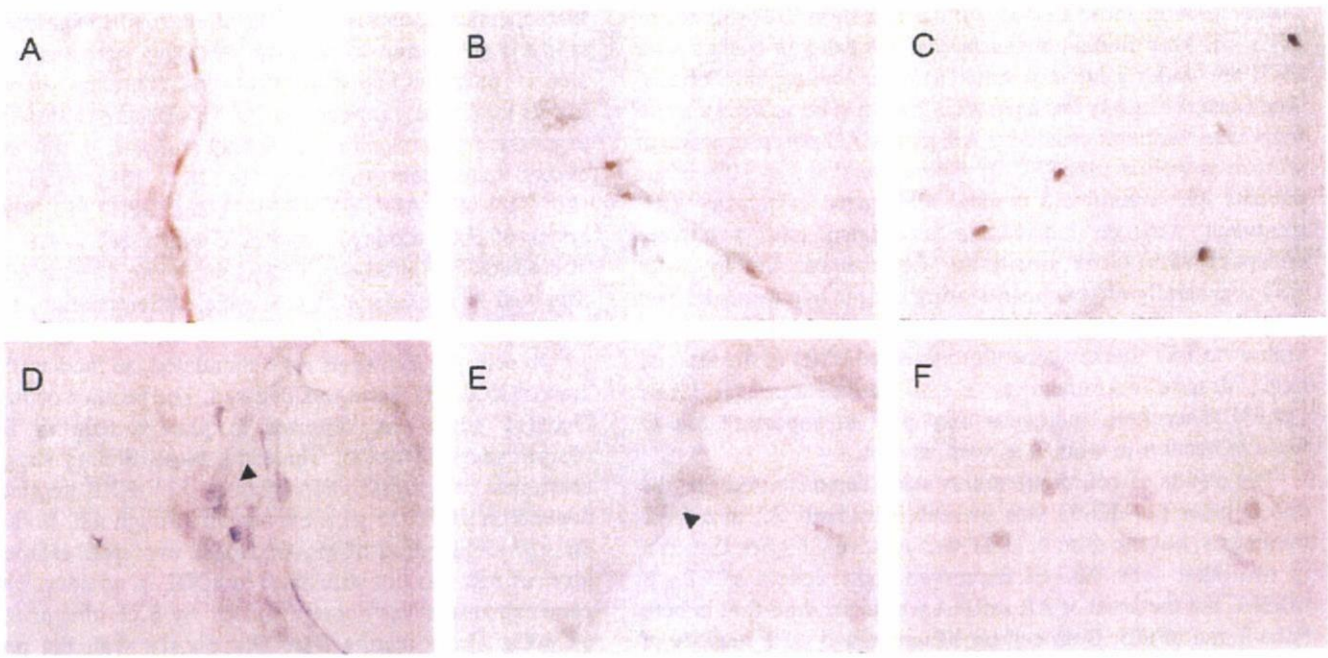

Fig. 8. Immunohistochemistry of androgen receptor in human bone tissues. Immunoreactivity of androgen receptor was detected in nuclei of osteoblasts/liner cells (A, B) but not in osteoclasts (D, E; arrowheads). Immunoreactivity of androgen receptor was also detected in nuclei of osteocytes (C) and condrocytes (F).

array analysis and following quantitative RT-PCR. COL1A1, SMAD5, and SPARC (osteonectine) were up-regulated by EXE and/or DHT treatments in both hFOB and Saos-2 cells. EXE or DHT treatments in both hFOB and Saos-2 also resulted in increased ALP activity. There have been, however, no studies reported on whether these genes are primary or secondary androgen responsive genes in osteoblasts. The AR-specific antagonist, OHF demonstrated no inhibitory effects on RUNX2 expression increased by EXE or DHT treatment in hFOB cells. In addition, hFOB cell growth induced by high dose of EXE treatment was not completely inhibited by OHF treatment. These results all suggest that EXE also may stimulate hFOB cell proliferation through both AR dependent and independent pathways. From our data of steroid production in hFOB, EXE may have an additional androgenic effect through increased TST levels in conjunction with inhibition of aromatization in hFOB cells. However, it awaits further investigations for clarification.

In normal bone remodeling, bone formation by osteoblasts follows bone resorption by osteoclasts and occurs in a precise and quantitative manner (coupling). In this coupling between bone formation and resorption, a coupling factor that induces bone formation is considered to be released during osteoclastic bone resorption [44]. This study has focused on the specific effects on osteoblast cells. However, it is true that there were significant increases in both serum bone formation and resorption markers in postmenopausal women administered with EXE for 2 years [26]. Osteoclasts, which are responsible for bone resorption, are target cells for many anti-osteoporosis therapeutic agents such as bisphosphonate of postmenopausal women [45]. However, it is unclear whether EXE acts on osteoclast directly. Chen et al. [46] reported that testosterone inhibited osteoclast formation stimulated by parathyroid hormone through the AR but not through the production of intrinsic estrogen using primary mouse osteoclast cells. In both human and rodent bone tissues, AR is expressed in both osteoblasts and osteocytes [47,48]. However, AR is detected in osteoclasts of rodent but not in human cells [31,47,48]. Therefore, in humans, androgens are considered to exert their effects on bone through osteoblasts. EXE may therefore exert its possible androgenic effects on human bone through osteoblasts but not osteoclasts. Results of our present study also suggest the possible roles of EXE on osteoblast cells through AR independent manner. Results of clinical studies suggest that the combination therapy of AI and COX-2 inhibitors could provide more effective aromatase inhibition than single therapy in hormone-sensitive postmenopausal breast cancer [49]. Bone resorption induced by IL-1 and IL-6 was also reported to occur via stimulation of COX-2 dependent PGE_2 production in osteoblasts *in vitro* [50]. Therefore, further investigations are required to clarify the effects of AI including EXE on human bone tissues.

In summary, this study using osteoblast and osteoblast-like cell lines suggested the potential protective effect of steroidal AI, EXE on osteoblasts occurred through both AR dependent and independent pathways. HOXD11 gene known as bone morphogenesis factor and osteoblast growth-related genes were induced by EXE treatment as well as DHT treatment in both hFOB and Saos-2. Damages of bone tissues by estrogen depletion caused by AI administration are considered unavoidable but the selection of potential hormone therapies which could minimize the damages or injuries of bone tissues is considered important.

Acknowledgments

We appreciate Dr. Shin-ichi Hayashi (Divisions of Molecular Medical Technology, Tohoku University School of Medicine) for critical comments. We also appreciate Ms. Chika Tazawa, Ms. Toshie Suzuki, Ms. Miki Mori and Mr. Katsuhiko Ono (Department of Pathology, Tohoku University School of Medicine) for skillful technical assistances. This research was supported by Grant-in-aid for Health and Labor Sciences Research Grant on Risk of Chemical Substances (H16-Kagaku-002) from Ministry of Health, Labor, and Welfare, Japan and Kanzawa Medical Research Foundation, Nagano, Japan.

References

[1] Rogers J. Estrogens in the menopause and postmenopause. N Engl J Med 1969;280:364–7.
[2] Wingate L. The epidemiology of osteoporosis. J Med 1984;15:245–66.
[3] Felson DT, Zhang Y, Hannan MT, Kiel DP, Wilson PW, Anderson JJ. The effect of postmenopausal estrogen therapy on bone density in elderly women. N Engl J Med 1993;329:1141–6.
[4] Lester L, Coleman R. Bone loss and the aromatase inhibitors. Br J Cancer 2005;93:S16–22.
[5] Miller WR, Dixon JM. Antiaromatase agents: preclinical data and neoadjuvant therapy. Clin Breast Cancer 2000;1:S9–S14.
[6] Lønning PE, Paridaens R, Thurlimann B, Piscitelli G, di Salle E. Exemestane experience in breast cancer treatment. J Steroid Biochem Mol Biol 1997;61:151–5.
[7] Center for Drug Evaluation and Research Application Number NDA 20753 (Exemestane) Medical Review. Food and Drug Administration, 1999.
[8] Goss PE, Qi S, Josse RG, Pritzker KPH, Mendes M, Hu H, et al. The steroidal Aromatase inhibitor exemestane prevent bone loss in ovariectomized rats. Bone 2004;34:384–92.
[9] Goss PE, Qi S, Cheung AM, Hu H, Mendes M, Pritzker KPH. Effects of steroidal aromatase inhibitor exemestane and the nonsteroidal aromatase inhibitor letrozole on bone and lipid metabolism in the ovariectomized rats. Clin Cancer Res 2004;10:5717–23.
[10] Sasano H, Uzuki M, Sawai T, Nagura H, Matsunaga G, Kashimoto O, et al. Aromatase in human bone tissue. J Bone Miner Res 1997;12:1416–23.
[11] Schweikert HU, Wolf L, Romalo G. Oestrogen formation from Androstendione in human bone. Clin Endocrinol 1995;43:37–42.
[12] Purohit A, Flanagan AM, Reed MJ. Estrogen synthesis by osteoblast cell lines. Endocrinology 1992;131:2027–9.
[13] Tanaka S, Haji M, Nishi Y, Yanase T, Takayanagi R, Nawata H. Aromatase activity in human osteoblast-like osteosarcoma cell. Calcif Tissue Int 1993;52:107–9.
[14] Recanatini M, Bisi A, Cavalli A, Belluti F, Gobbi S, Rampa A, et al. A new class of nonsteroidal aromatase inhibitors: design and synthesis of chromone and xanthone derivatives and inhibition of the P450 enzymes aromatase and 17 alpha-hydroxylase/C17,20-lyase. J Med Chem 2001;44:672–80.
[15] Linkhart TA, Mohan S, Baylink DJ. Growth factors for bone growth and repair: IGF, TGF beta and BMP. Bone 1996;19:1S–12S.
[16] Harris SA, Enger RJ, Riggs BL, Spelsberg TC. Development and characterization of a conditionally immortalized human fetal osteoblastic cell line. J Bone Miner Res 1995;10:178–86.
[17] Suzuki T, Darnel AD, Akahira JI, Ariga N, Ogawa S, Kaneko C, et al. 5alpha-reductases in human breast carcinoma: possible modulator of in situ androgenic actions. J Clin Endocrinol Metab 2001;86:2250–7.

[18] Miki Y, Suzuki T, Tazawa C, Ishizuka M, Semba S, Gorai I, et al. Analysis of gene expression induced by diethylstilbestrol (DES) in human primitive Müllerian duct cells using microarray. Cancer Lett 2005;220:197–210.
[19] Yamamoto M, Takahashi Y, Tabata Y. Controlled release by biodegradable hydrogels enhances the ectopic bone formation of bone morphogenetic protein. Biomaterials 2003;24:4375–83.
[20] Kanno J, Aisaki K, Igarashi K, Nakatsu N, Ono A, Kodama Y, et al. "Per cell" normalization method for mRNA measurement by quantitative PCR and microarrays. BMC Genomics 2006;29:64.
[21] Eisen MB, Spellman PT, Brown PO, Bostein D. Cluster analysis and display of genome-wide expression patterns. Proc Natl Acad Sci U S A 1998;95:14863–8.
[22] Miki Y, Nakata T, Suzuki T, Darnel AD, Moriya T, Kaneko C, et al. Systemic distribution of steroid sulfatase and estrogen sulfotransferase in human adult and fetal tissues. J Clin Endcrinol Metab 2002;87:5760–8.
[23] Ishizuka M, Hatori M, Suzuki T, Miki Y, Darnel AD, Tazawa C, et al. Sex steroid receptors in rheumatoid arthritis. Clin Sci (Lond) 2004;106: 293–300.
[24] Rodan GA, Noda M. Gene expression in osteoblastic cells. Crit Rev Eukaryot Gene Expr 1991;1:85–98.
[25] Ito Y, Miyazono K. RUNX transcription factors as key role of TGF-β superfamily signaling. Curr Opin Genet Dev 2003;13:43–7.
[26] Lønning PE, Geisler J, Krag LE, Erikstein B, Bremnes Y, Hagen AI, et al. Effects of exemestane administered for 2 years versus placebo on bone mineral density, bone biomarkers, and plasma lipids in patients with surgically respected early breast cancer. J Clin Oncol 2005;23:4847–9.
[27] Coombes RC, Hall E, Gibson LJ, Paridaens R, Jassem J, Delozier T, et al. Intergroup Exemestane Study. A randomized trial of exemestane after two to three years of tamoxifen therapy in postmenopausal women with primary breast cancer. N Engl J Med 2004;350:1081–92.
[28] Coleman RE, Banks LM, Girgis SI, Vrdoljak E, Fox J, Porter LS, et al. Skeletal effect of exemestane in the Intergroup Exemestane Study (IES)—2 years bone mineral density (BMD) and bone biomarker data. Breast Cancer Res Treat 2005;94:S233.
[29] Vottero A, Stratalis CA, Ghizzoni L, Longui CA, Karl M, Chrousos GP. Androgen receptor-mediated hypersensitivity to androgen in women with nonhyperandrogenic hirsutism: skewing of X-chromosome inactivation. J Clin Endocrinol Metab 1999;84:1091–5.
[30] Brum IS, Spritzer PM, Paris F, Maturana MA, Audran F, Sultan C. Association between androgen receptor gene CAG repeat polymorphism and plasma testosterone levels in postmenopausal women. J Soc Gynecol Investig 2005;12:135–41.
[31] Vanderschueren D, Vandenput L, Boonen S, Lindberg MK, Bouillon R, Ohlsson C. Androgens and bone. Endocr Rev 2004;25:389–425.
[32] Turner A, Chen T, Barber T, Malabanan A, Holick M, Tangpricha V. Testosterone increases bone mineral density in female-to-male transsexuals: a case series of 15 subjects. Clin Endocrinol (Oxf) 2004;61:560–6.
[33] Ruetsche AG, Kneubuehl R, Birkhaeuser MH, Lippuner K. Cortical and trabecular bone mineral density in transsexuals after long-term cross-sex hormonal treatment: a cross-sectional study. Osteoporos Int 2005;16: 791–98.
[34] Kasperk CH, Wergedal JE, Farley JR, Linkhart TA, Turner RT, Baylink DJ. Androgens directly stimulate proliferation of bone cells in vitro. Endocrinology 1989;124:1576–8.
[35] Kasperk C, Fitzsimmons R, Strong D, Mohan S, Jennings J, Wergedal J, et al. Studies of the mechanism by which androgens enhance mitogenesis and differentiation in bone cells. J Clin Endocrinol Metab 1990;71:1322–9.
[36] Chen Q, Kaji H, Kanatani M, Sugimoto T, Chihara K. Testosterone increases osteoprotegerin mRNA expression in mouse osteoblast cells. Horm Metab Res 2004;36:674–8.
[37] Bord S, Horner A, Beavan S, Compston J. Estrogen receptors alpha and beta are differentially expressed in developing human bone. J Clin Endocrinol Metab 2001;86:2309–14.
[38] Sala A, Watson R. B-Myb protein in cellular proliferation, transcription control, and cancer: latest developments. J Cell Physiol 1999;179:245–50.
[39] Chalhoub N, Benachenhou N, Rajapurohitam V, Pata M, Ferron M, Frattini A, et al. Grey-lethal mutation induces severe malignant autosomal recessive osteopetrosis in mouse and human. Nat Med 2003;9:399–406.
[40] Boulet AM, Capecchi MR. Multiple roles of Hoxa11 and Hoxd11 in the formation of the mammalian forelimb zeugopod. Development 2004; 131:299–309.
[41] Lundberg P, Lundgren I, Mukohyama H, Lehenkari PP, Horton MA, Lerner UH. Vasoactive intestinal peptide (VIP)/pituitary adenylate cyclase-activating peptide receptor subtypes in mouse calvarial osteoblasts: presence of VIP-2 receptors and differentiation-induced expression of VIP-1 receptors. Endocrinology 2001;142:339–47.
[42] Gutierrez J, Osses N, Brandan E. Changes in secreted and cell associated proteoglycan synthesis during conversion of myoblasts to osteoblasts in response to bone morphogenetic protein-2: role of decorin in cell response to BMP-2. J Cell Physiol 2006;206:58–67.
[43] Omi M, Fisher M, Maihle NJ, Dealy CN. Studies on epidermal growth factor receptor signaling in vertebrate limb patterning. Dev Dyn 2005;233:288–300.
[44] Rodan GA, Raisz LG, Bilezikian JP. Pathophysiology of osteoporosis. . (chapter 73)In: Bilezikian JP, Raisz LG, Rodan GA, editors. Principles of bone biology, 2nd ed., vol. 1. NY, USA: Academic Press, A division of Harcourt, Inc.; 2002. p. 1275–90.
[45] Kellinsalmi M, Monkkonen H, Monkkonen J, Leskela HV, Parikka V, Hamalainen M, et al. In vitro comparison of clodronate, pamidronate and zoledronic acid effects on rat osteoclasts and human stem cell-derived osteoblasts. Basic Clin Pharmacol Toxicol 2005;97:382–91.
[46] Chen Q, Kaji H, Sugimoto T, Chihara K. Testosterone inhibits osteoclast formation stimulated by parathyroid hormone through androgen receptor. FEBS Lett 2001;491:91–3.
[47] Abu EO, Horner A, Kusec V, Triffitt JT, Compston JE. The localization of androgen receptors in human bone. J Clin Endocrinol Metab 1997; 82:3493–7.
[48] Wiren KM, Orwoll ES. Androgens: receptor expression and steroid action in bone. . (chapter 43)In: Bilezikian JP, Raisz LG, Rodan GA, editors. Principles of bone biology, 2nd ed., vol. 1. NY, USA: Academic Press, A division of Harcourt, Inc.; 2002. p. 757–72.
[49] Chow LW, Wong JL, Toi M. Celecoxib anti-aromatase neoadjuvant (CAAN) trial for locally advanced breast cancer: preliminary report. J Steroid Biochem Mol Biol 2003;86:443–7.
[50] Sato T, Morita I, Sakaguchi K, Nakahama KI, Smith WL, Dewitt DL, et al. Involvement of prostaglandin endoperoxide H synthase-2 in osteoclast-like cell formation induced by interleukin-1 beta. J Bone Miner Res 1996;11:392–400.

Hypothalamus Region-Specific Global Gene Expression Profiling in Early Stages of Central Endocrine Disruption in Rat Neonates Injected with Estradiol Benzoate or Flutamide

Makoto Shibutani,[1] Kyoung-Youl Lee,[1]* Katsuhide Igarashi,[2] Gye-Hyeong Woo,[1] Kaoru Inoue,[1] Tetsuji Nishimura,[3] Masao Hirose[1]

[1] Division of Pathology, National Institute of Health Sciences, Setagaya-ku, Tokyo 158-8501, Japan

[2] Division of Molecular Toxicology, National Institute of Health Sciences, Setagaya-ku, Tokyo 158-8501, Japan

[3] Division of Environmental Chemistry, National Institute of Health Sciences, Setagaya-ku, Tokyo 158-8501, Japan

Received 3 February 2006; revised 8 September 2006; accepted 14 September 2006

ABSTRACT: To identify genes linked to early stages of disruption of brain sexual differentiation, hypothalamic region-specific microarray analyses were performed using a microdissection technique with neonatal rats exposed to endocrine-acting drugs. To validate the methodology, the expression fidelity of microarrays was first examined with two-round amplified antisense RNAs (aRNAs) from methacarn-fixed paraffin-embedded tissue (PET) in comparison with expression in unfixed frozen tissue (UFT). Decline of expression fidelity when compared with the 1×-amplified aRNAs from UFTs was found as a result of the preferential amplification of the 3′ side of mRNAs in the second round *in vitro* transcription. However, expression patterns for the 2×-amplified aRNAs were mostly identical between methacarn-fixed PET and UFT, suggesting no obvious influence of methacarn fixation and subsequent paraffin embedding on expression levels. Next, in the main experiment, neonatal rats at birth were treated subcutaneously either with estradiol benzoate (EB; 10 μg/pup) or flutamide (FA; 250 μg/pup), and medial preoptic area (MPOA)-specific microarray analysis was performed 24 h later using 2×-amplified aRNAs from methacarn-fixed PET. Numbers of genes showing constitutively high expression in the MPOA predominated in males, implying a link with male-type growth supported by perinatal testosterone. Around 60% of genes showing sex differences in expression demonstrated altered levels after EB treatment in females, suggesting an involvement of genes necessary for brain sexual differentiation. When compared with EB, FA affected a rather small number of genes, but fluctuation was mostly observed in females, as with EB. Moreover, many selected genes common to EB and FA showed down-regulation in females with both drugs, suggesting a common mechanism for endocrine center disruption in females, at least at early stages of post-natal development. Develop Neurobiol 67: 253–269, 2007

Keywords: brain sexual differentiation; microarray; estradiol benzoate; flutamide; microdissection

Present address: Toxicological Research Team, Occupational Safety and Health Research Institute, 104-8, Munji-Dong, Yuseong-Gu, Daejeon, 305-380, Korea.

Correspondence to: M. Shibutani (shibutan@nihs.go.jp).

Contract grant sponsors: Ministry of the Environment, Ministry of Health, Labor and Welfare of Japan.

Published online 3 January 2007 in Wiley InterScience (www.interscience.wiley.com).
DOI 10.1002/dneu.20349

INTRODUCTION

Sex steroids play important roles in sexual differentiation of the mammalian brain (McEwen and Alves, 1999). In the rat, there is a critical period beginning

at the last week of gestation and terminating in few days after birth, during which circulating testosterone secreted from the fetal and neonatal testes masculinizes the brain in males (Rhees et al., 1990a,b), the hormone being metabolized to estradiol by the enzyme aromatase to trigger brain sexual differentiation. Steroid-mediated processes during this period, including alterations in neuronal plasticity, myelination, and cell death, are the basis of sexual dimorphism in the structure and function of the adult brain (Matsumoto et al., 2000). For example, the medial preoptic area (MPOA) in the hypothalamus that is believed to mediate sexually dimorphic behavior in adult life (Meisel and Sachs, 1994; Numan, 1994) contains a highly cellular region, the sexually dimorphic nucleus of preoptic area (SDN-POA), that has an approximately 10 times larger volume in males than in females (Meredith et al., 2001). Inhibitory effects of steroids against the normal apoptosis that proceeds in the female SDN-POA during the critical period have been suggested to be responsible for the large size in males (Arai et al., 1996; Davis et al., 1996).

Sex steroids with their receptors are powerful regulators of gene transcription, and changes in the hormonal milieu during development can trigger reproductive dysfunction in later life by affecting molecular cascades responsible for sexual differentiation (McEwen and Alves, 1999). For instance, both α and β estrogen receptors (ERs) are strongly expressed in the hypothalamus during neonatal development, showing region-specific distributions (Orikasa et al., 2002), and neonatal hormonal manipulations can affect their expression levels and/or locations (Tena-Sempere et al., 2001; Orikasa et al., 2002), resulting in organizational changes in the brain structure and reproductive function in later life (Nagao et al., 1999; Tsukahara et al., 2003).

To elucidate mechanisms underlying disruption of brain sexual differentiation, gene screening applying global gene expression profiling in target brain region(s) is an effective approach. We recently established multipurpose genetic analysis methods with paraffin-embedded tissues (PETs) utilizing methacarn as a novel fixation tool, in combination with laser microbeam microdissection (Shibutani et al., 2000; Shibutani and Uneyama, 2002; Uneyama et al., 2002). With this system, we could achieve high performance regarding quantitative expression analysis of mRNAs using real-time RT-PCR, close to that with unfixed frozen tissue (UFT) (Takagi et al., 2004).

In the present study, we focused on region-specific gene expression analysis utilizing microarrays to identify genes linked with disruption of brain sexual differentiation in rats. With limited tissue samples, such as those collected by microdissection, multi-round amplification of mRNAs is necessary to obtain sufficient quantities of antisense RNAs (aRNAs) applicable for microarray analysis, and therefore, we first performed validation experiments using methacarn-fixed liver PETs to determine fidelity of expression profiles with 2× *in vitro* transcribed aRNAs in comparison with 1×- or 2×-amplified examples from UFTs. After confirmation of the efficacy of the methods, we then analyzed gene expression profiles in the neonatal MPOA in terms of sex differences and acute responses to neonatally injected estradiol benzoate (EB), a potent analog of endogenous estrogen, or flutamide (FA), a non-steroidal anti-androgen.

METHODS

Chemicals and Animals

Estradiol benzoate (EB; CAS# 50-50-0) and flutamide (FA; CAS# 13311-84-7) were purchased from Sigma (St. Louis, MO), sodium phenobarbital (PB; CAS# 57-30-7) from Wako Pure Chemical Industries (Osaka, Japan) and CD^{R}(SD)IGS rats from Charles River Japan (Kanagawa, Japan). For the preliminary validation study regarding expression fidelity with microarrays using methacarn-fixed PET, one 7-week-old male rat was used, and for gene expression profiling in the early stage of disruption of brain sexual differentiation, six pregnant rats at gestational Day 3 (the day when vaginal plugs were observed was designated as GD 0). The animals were housed individually in polycarbonate cages (SK-Clean, 41.5 × 26 × 17.5 cm in size; CLEA Japan, Tokyo) with wood bedding (Soft Chip; Sankyo Lab Service, Tokyo, Japan), maintained in an air-conditioned animal room (temperature: 24°C ± 1°C, relative humidity: 55% ± 5%) with a 12-h light–dark cycle, and allowed *ad libitum* access to feed and tap water. For the rat in the preliminary validation study, CRF-1, a standard rodent diet, purchased from Oriental Yeast Co. (Tokyo, Japan), was used as the basal diet. For pregnant animals, soy-free diet (Oriental Yeast Co.) was used as a basal diet to remove possible interaction of phytoestrogens included in the regular soy-containing diet with the action of EB or FA. The formulation of the soy-free diet as well as the dietary concentrations of estrogens and phytoestrogens were as described earlier (Masutomi et al., 2003). Essentially, concentrations of phytoestrogens except for coumestrol, detected at 0.3 mg/100 g diet, were lower than the detection limit (0.05 mg/100 g diet).

Experimental Design

In the preliminary validation study, the rat received PB intraperitoneally at 80 mg/kg, once daily for three days. The dose was selected according to the PB-specific enzyme

induction protocol described by Kocarek et al. (1998). One day after the last injection, the animal was killed by exsanguination from the abdominal aorta under ether anesthesia, and the liver was removed and trimmed to make tissue blocks sized 5 × 5 × 3 mm.

For gene expression profiling in the early stage of disruption of brain sexual differentiation, offspring of two dams each were injected subcutaneously either with EB, FA, or vehicle at postnatal day (PND) 1 (the day of delivery) within 3–6 h after completion of delivery. The dose level of EB was set as 10 μg/pup, shown in our laboratory, to induce typical estrogenic effects on sexual development and the endocrine/reproductive system at the adult stage in both sexes, including reduction of the SDN volume in males (Shibutani et al., 2005). For FA, 250 μg/pup was selected on the basis of earlier study finding of retardation of male reproductive development with repeated injections of this dose (Rivas et al., 2002). Each chemical was dissolved in sesame oil to achieve a total injection volume of 20 μL. Vehicle control animals were injected with 20 μL of sesame oil. Twenty-four hours after the injection (PND 2), offspring including vehicle control pups were killed by decapitation for removal of brains.

The animal protocols were reviewed and approved by the Animal Care and Use Committee of the National Institute of Health Sciences, Japan.

Preparation of Tissue Specimens and Microdissection

Liver tissues of the rat treated with PB were either quick frozen in ethanol–dry ice after embedding in Tissue-Tek 4583 OCT compound (Sakura Finetek Japan, Tokyo, Japan), or immersed in methacarn for tissue fixation. For this purpose, methacarn solution consisting of 60% (vol/vol) absolute methanol, 30% chloroform, and 10% glacial acetic acid was freshly prepared and stored at 4°C (Shibutani et al., 2000; Shibutani and Uneyama, 2002; Takagi et al., 2004), before fixation for 2 h at 4°C. Fixed tissue samples were then dehydrated three times for 1 h in fresh 99.5% ethanol at 4°C, immersed in xylene once for 1 h and then three times for 30 min at room temperature, and immersed in hot paraffin (60°C) four times for 1 h, for a total of 4 h. Both UFTs (n = 3) and methacarn-fixed PETs (n = 3) were sectioned at 10 μm and 20 sections per block were stored in 1.5 mL tubes at −80°C until RNA extraction.

For MPOA-specific microarray analysis, whole brains of rat pups were subjected to methacarn fixation (n = 3/sex/group). Before embedding, coronal brain slices including the hypothalamus were trimmed. Microdissection of the MPOA was performed based on the method described earlier (Takagi et al., 2004). After paraffin embedding, 6-μm-thick sections between three 18-μm-thick sections were prepared. The 18-μm sections were mounted onto PEN-foil film (Leica Microsystems, Tokyo, Japan) overlaid on glass slides, dried in an incubator overnight at 37°C, deparaffinized with xylene three times each for 3 min, placed in 99.5% ethanol for 1 min, and then air-dried. The localization of the SDN-POA, identified as an intensely stained cellular region, was determined by microscopic observation of the 6-μm-thick sections stained with hematoxylin and eosin (HE) (as shown in Fig. 1), and bilateral portions of the MPOA (500 × 300 μm) containing SDN-POA were microdissected from the adjacent unstained 18-μm-thick sections using PALM Robot-MicroBeam equipment (Carl Zeiss Co., Tokyo, Japan). In both sexes, 10–12 sections from one animal were used for microdissection, and the microdissected samples were stored in one 1.5 mL sample tube at −80°C until extraction of total RNA.

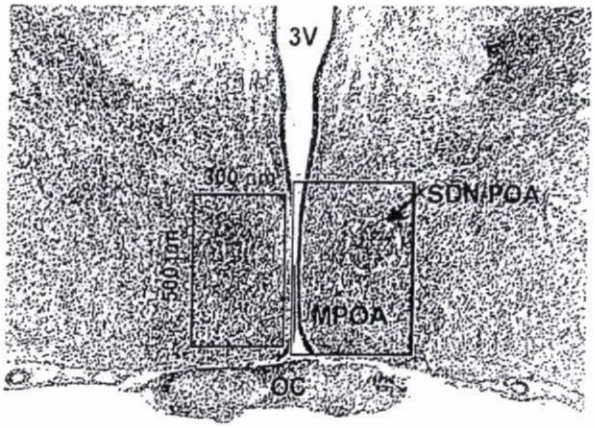

Figure 1 Overview of the hypothalamic MPOA at PND 2. Bilateral portions of MPOA as shown in the left boxed area were microdissected from sections of methacarn-fixed paraffin-embedded brain slices for gene expression analysis. The right boxed area is the anatomical location for immunohistochemical observation of protein signals shown in Table 6 and Fig. 6 (3V, third ventricle; SDN-POA, sexually dimorphic nucleus of the preoptic area; MPOA, medial preoptic area; OC, optic chiasm).

RNA Isolation, Amplification, and Microarray Analysis

Total RNAs from liver sections of UFTs and methacarn-fixed PETs were extracted with RNeasy® Mini (QIAGEN, Hilden, Germany) according to the manufacturer's protocol, with the final elution volume set at 30 μL. Contaminating genomic DNA was digested with DNase I (Ambion, Austin, TX) at the end of the extraction. Total RNAs from microdissected MPOAs were extracted using an RNAqueous®-Micro RNA isolation kit (Ambion), eluted twice with a total volume of 14 μL, and then treated with DNase according to the manufacturer's protocol.

For quantitation of RNA yield, 1 μL of isolated RNA was labeled with a RiboGreen™ RNA Quantitation kit (Molecular Probes, Eugene, Oregon) and concentrations were estimated with a fluorescence spectrophotometer F2500 (Hitachi Co., Tokyo, Japan) in 1 mL of total volume with water.

For microarray analysis, extracted total RNA samples were subjected to amplification, consisting of reverse tran-

scription and subsequent *in vitro* transcription, using a MessageAmp™ aRNA Kit (Ambion) with an oligo dT/T7 primer, according to the manufacturer's protocol. Total RNA samples from liver UFT sections were either subjected to one- or two-step amplification, and those from methacarn-fixed liver PET sections were subjected to two-step amplification. For expression analysis with the microdissected MPOA, two-step amplification was performed. For one-step amplification, 5 μg of total RNA was subjected to one-round of aRNA amplification. For the two-step amplification, 50 ng of total RNA was subjected to first-round amplification, and resultant aRNAs of 150–200 ng were subjected to second-round amplification. During the second *in vitro* transcription, generating aRNAs were labeled with biotin-UTP and biotin-CTP (Enzo Biochem, Farmingdale, NY).

For normalization of transcript levels with reference to amplification efficiency, an *in vitro* transcribed spike RNA from pGIBS-PHE (American Type Culture Collection, Manassas, VA), a short fragment of *Bacillus subtilis* (accession no. M24537 in GenBank/EMBL data bank), was added to the extracted total RNA at 3.76 pg/μg.

After the second-round amplification, 20 μg of biotinylated aRNA was denatured at 94°C for 35 min in fragmentation buffer (4×10^{-2} *M* Tris-acetate, pH 8.1, 1×10^{-7} *M* KOAc, 3×10^{-2} *M* MgOAc) and subjected to hybridization in a mixture containing control cRNAs (Affymetrix, Santa Clara, CA). Aliquots of 200 μL containing approximately 15 μg of aRNA were hybridized with GeneChip® Rat Genome U34A Arrays (Affymetrix) at 45°C for 18 h, stained with streptavidin/R-phycoerythrin conjugates (Molecular Probes), and then scanned with a GeneChip® Scanner 3000 (Affymetrix). Individual samples were subjected to analysis with individual microarrays in both the validation study and the MPOA-specific gene expression profiling study (n = 3/group for comparison in each study).

Real-Time RT-PCR

Quantitative real-time RT-PCR was performed for confirmation of expression values obtained with microarrays using ABI Prism 7700 (Applied Biosystems Japan, Tokyo, Japan). In a separate microarray study, to investigate gene expression changes in microdissected MPOA of rat neonates that have been administered 0.01–0.5 ppm ethinylestradiol through the maternal diet, we selected two genes, i.e., thymosin β4 and GTP-binding protein (Gαi2), showing profound sex differences in basal expression. Gene specific primers for thymosin β4 (accession no. NM_031136 in the GenBank/EMBL data banks) and Gαi2 (M12672) as well as corresponding TaqMan® MGB probes (6-FAM™-dye-labeled) were obtained from Assays-on-Demand™ Gene Expression Products (Applied Biosystems Japan). Reverse transcription was performed using 100 ng of first-round aRNAs prepared for microarray analysis containing spike RNA with a high-capacity cDNA Archive Kit (Applied Biosystems Japan) in a 100 μL total reaction volume. Real-time PCR was performed in a 50 μL reaction volume using the TaqMan probe detection system with 25 μL of TaqMan® Universal PCR Master Mix (Applied Biosystems Japan) and 2.5 μL each of target primer mix and RT product. Cycle parameters with this system were: single step of 50°C for 2 min, initial activation at 95°C for 10 min, 45 cycles of 15 sec at 95°C, and 60 sec at 60°C. For quantitation of expression data, a standard curve method was applied using first-round amplified aRNAs from a male MPOA as a standard sample.

For the spike gene (*Bacillus subtilis*), *in vitro* amplified transcript levels were measured by one-step real-time RT-PCR using the SYBR® Green detection system in a 50 μL total reaction mixture containing 25 μL of 2× QuantiTect™ SYBR® Green PCR Master Mix (QIAGEN), 8 ng of first-round amplified aRNA, multiscribe RTase (17.5 units), RNase inhibitor (20 units), and 2.5×10^{-7} *M* of primers. Cycle parameters in this system were as follows: 48°C for 30 min, 95°C for 10 min, 45 cycles of 15 sec at 95°C, and 60 sec at 60°C. The primer set for the spike gene, 5′-AGCGCCCCGGACTGA-3′ (forward; nucleotides 3152–3166), and 5′-CTCTAGGCCCAAAACGACCTT-3′ (reverse; nucleotides 3107–3127), was designed using Primer Express® software (Version 2.0; Applied Biosystems Japan).

Immunohistochemical Analysis

Whole brains of male and female neonates injected with EB or vehicle at PND 1 and obtained on PND 2 were subjected to fixation in Bouin's solution overnight (n = 4/sex/group). Coronal brain slices including the hypothalamus were trimmed and paraffin-embedded, and 3-μm serial sections were prepared for localization of the MPOA including the SDN-POA with HE-stained sections each one prepared in every 10 sections.

Immunohistochemistry was performed with antibodies against poly(ADP-ribose) polymerase (PARP) (rabbit IgG, 50× dilution; Santa Cruz Biotechnology, Santa Cruz, CA), glutamate receptor (GluR) 1 (rabbit immunoaffinity purified IgG, 1 μg/mL; Upstate, Charlottesville, VA), GluR5 (rabbit polyclonal IgG, 100× dilution; Upstate), GluR6/7 (rabbit immunoaffinity purified IgG, 5 μg/mL; Upstate), microtubule-associated protein (MAP) 2 (mouse monoclonal IgG_1, 400× dilution; Chemicon International, Inc, Temecula, CA), and metallothionein-1/2 (MT-1/2; clone E9, mouse $IgG_{1\kappa}$, 400× dilution; DakoCytomation, Carpinteria, CA). The PARP antibody can detect PARP-1, and to a lesser extent PARP-2, according to the manufacturer's product information. For detection of GluR1, GluR5, and GluR6/7, deparaffinized sections were subjected to microwave treatment, four times for 3 min in 1×10^{-2} *M* citrate buffer (pH 6.0), according to the recommendation in the manufacturer's protocol. For MAP2, microwave treatment was performed twice for 3 min in the same citrate buffer. Nonspecific endogenous peroxidase activity was blocked by treatment with 0.9% hydrogen peroxide in absolute methanol for 10 min. After masking with normal goat (for rabbit polyclonal antibodies) or horse (for mouse monoclonal antibod-